NONINVASIVE IMAGING OF CAROTID ARTERIAL STRAIN USING DISPLACEMENT-ENCODED MRI

Thesis by

Alexander P. Lin

In Partial Fulfillment of the Requirements

for the Degree of

Doctor of Philosophy

California Institute of Technology

Pasadena, California

2009

(Defended February 24th, 2009)

Acknowledgements

"…nos esse quasi nanos, gigantium humeris insidentes, ut possimus plura eis et remotiora videre, non utique proprii visus acumine, aut eminentia corporis, sed quia in altum subvenimur et extollimur magnitudine gigantean…"

("…we are like dwarfs on the shoulders of giants, so that we can see more than they, and things at a greater distance, not by virtue of any sharpness of sight on our part, or any physical distinction, but because we are carried high and raised up by their giant size.")

—Bernard of Chatres, attributed by John of Salisbury, 1159 in Metalogicon

It would seem only appropriate that even the great Sir Isaac Newton based his famous quote on earlier work by others. I have been very fortunate to have had the opportunity to work with the top scientists in their field during my PhD training. This thesis would not have been possible without the guidance of the following "giants": I would like to thank my thesis advisor, Dr. Scott Fraser, for providing me with a home for my research at Caltech in Fraserlab and the Caltech Brain Imaging Center. His constant support and the freedom pursue my interests will always be greatly appreciated. I am also grateful for the opportunities that my thesis committee chairman, Dr. Morteza Gharib, has given me at Caltech as well as the excellent advice that he and the other members of my thesis committee, Dr. Paul Patterson, and Dr. J. Michael Tyszka have provided. I am especially grateful to Dr. Han Wen (NHLBI/NIH) for his support in so many aspects of this thesis. He not only provided me with the opportunity to spend time at the National Institutes of Health, a wonderful learning experience in itself, but also purchased additional hardware

for the project and most importantly has been extremely generous with his time and effort teaching me and guiding me throughout my PhD experience. Finally, I would also like to thank Dr. Brian Ross who has mentored me since the very beginning over 12 years ago at Huntington Medical Research Institutes. His continued support and access to the MRI scanners at Huntington Hospital was much appreciated.

I have also had the great opportunity to give back to the scientific community by being a mentor to several undergraduate students through Caltech and the American Heart Association Summer Undergraduate Fellowship program at HMRI. I am very grateful for the help and efforts of Jessica Bastiannsen (Eindhoven University, Netherlands), Lauren Wisk (UCLA), Ajay Ullal (UCLA), Peter Bruno (UCSD), and Bryan Ching (UCSB). My interactions with the members of Fraserlab and Gharib lab have always been valuable and unfortunately too numerous to list. I greatly appreciated the support and efforts of the staff and students at the Caltech Brain Imaging Center: Mary Martin, Steve Flaherty, Ralph Lee, Daniel Procissi, Thomas Ng, and Lin Zhao. I would also like to thank the clinical MR team at HMRI: Thao Tran, Victor Xu, and Napapon Sailasuta for their assistance as well.

Last but not least, I am most grateful for the support of my family. My parents and in-laws have been always supportive of my endeavors and I appreciate their assistance and confidence in me. I would like to dedicate this thesis to the two ladies in my life: my wife Amy Lin whose unwavering support and tremendous patience with my career means more to me than she can possibly know and my daughter Ariel for whom I must now prepare my shoulders for her to stand.

Abstract

Stroke is the leading cause of disability in the United States and the third leading cause of death. These "brain attacks" occur when atherosclerosis, the progressive process of thickening and hardening of arterial walls, develops in the carotid arteries, leading to stenosis or thrombosis that cuts off the vital supply of blood and oxygen to the brain. These atherosclerotic plaques have been shown to form in regions of excessive stretching or strain. Furthermore, intravenous ultrasound studies (IVUS) have demonstrated that strain plays a role in determining those plaques most likely to rupture, the so-called vulnerable plaques. However, IVUS is an invasive technique that poses risks for patients and requires specialized methods that are not readily available in most hospitals. Therefore, the objective of this thesis is to develop a noninvasive method of measuring strain in the carotid artery that may provide an early diagnosis of stroke.

Magnetic resonance imaging (MRI) is a powerful noninvasive method of imaging the human body. An MRI technique called displacement encoding with stimulated echoes, or DENSE-MRI, has been shown to accurately measure strain in the human heart. This thesis describes the adaptation of the DENSE-MRI technique to the carotid arteries, validation and optimization of the DENSE-MRI pulse sequence, and *in vivo* strain measurements in human subjects. The results show the successful adaptation of this method in the carotid arteries and that strain measurements are accurate, reproducible, and robust. In particular, utilization of a single-shot pulse sequence effectively removes flow-sensitive artifacts that permit strain mapping at the bifurcation and in the internal and external carotid arteries, areas where plaque is most likely to form. Furthermore, it is shown that strain changes with age and may be a more sensitive diagnostic measure as patients with atherosclerosis show significantly lower strain values.

The primary contributions of this thesis are the achievement of quantitative measurements of strain in the carotid arteries and the development of a robust method of measuring strain in atherosclerosis that may facilitate the early diagnosis of stroke so that treatment can be provided before the devastating effects of the disease can take their course.

Table of Contents

Chapter 1: Prologue

Introduction

Stroke is the leading cause of serious, long-term disability in the United States with over 700,000 cases each year of which nearly 40% of these "brain attacks" result in death, making it the third leading cause of death [1]. The most common cause of stroke is the formation of atherosclerotic plaques in the carotid arteries that can grow large enough to block the flow of blood through the vessel (stenosis) or rupture causing blood clots (thrombosis) to form in the arteries that supply blood and oxygen to the brain [2] as shown in figure 1.1. One of the greater medical challenges is to identify the so-called "vulnerable plaque" that represents 70% of the culprit lesions that rupture [3]. Changes in arterial wall strain associated with this process have been demonstrated at several levels: molecular, mechanical, and clinical.

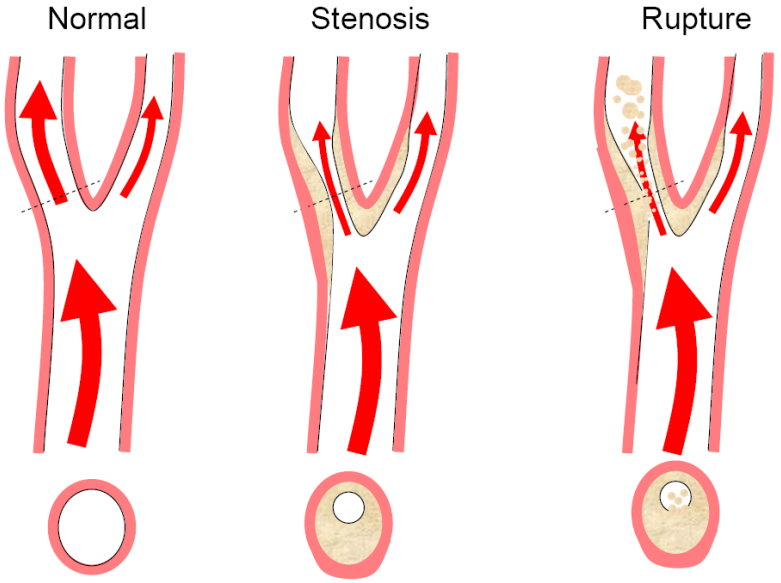

Figure 1.1. Carotid arteries and atherosclerosis. Top: Side view of the carotids showing blood flow (arrows) and reference for cross-sectional view (dotted line). Bottom: Cross-sectional view of the carotids.

Cyclic mechanical strain in blood vessels arises from the pulsatile nature of blood flow. It is the radial force that counteracts the effects of intraluminal blood pressure and has been shown in numerous studies to activate biochemical pathways that lead to the formation of atherosclerotic plaque, otherwise known as atherogenesis. Several studies have shown that cyclic strain induces the formation of reactive oxygen species (ROS) [4-7] that when overproduced results in injury to the vascular endothelium from oxidative stress. When endothelial cells undergo mechanical strain, NAD(P)H oxidase is upregulated [8] and is the likely source for ROS production. ROS acts as signal transduction agents in the activation of the NF-kB pathway, which leads to an increase cell adhesion molecule (CAM) expression [9]. CAM expression is key to atherogenesis because it attracts monocytes to the endothelial surface that transmigrate into the endothelium where they proliferate and differentiation into macrophages which eventually die and result in the lipid-filled contents of the atherosclerotic plaque [10]. It has been shown that CAM expression linearly increases with the amount of strain [11]. Vascular smooth muscle cells and fibroblasts are also influenced by cyclic strain, facilitating migration to the plaque and form the fibrous cap that covers the lesion [12]. As the plaque grows, vascular remodeling occurs in an effort to reduce the strain in the vascular wall which leads to narrowing of the inner diameter of the blood vessel, otherwise known as stenosis [13]. While there are certainly influences from other factors such as wall sheer stress, these studies show that cyclic strain is a key element of atherogenesis and therefore is the focus of this thesis.

DeBakey, Lawrie, and Glaser first showed in 1985 that atherosclerotic plaques tended to form in the carotid arteries showing rapid rate of progression and increased likelihood to be linked to occlusive disease in other parts of the body [14]. However, the

importance of the study was the first epidemiological evidence that atherosclerosis tended to form at bifurcations of the major arteries. This lead to many studies using finite-element analysis and computational fluid dynamics for the exploration of atherogenesis [15]. Biomechanical models derived from high-resolution IVUS [16-18] and MRI [19, 20] images showed that high strain can be found at regions of the carotid bifurcation that correlate with sites of early atherosclerotic inflammation [20]. Focal regions of high strain in the fibrous cap not only correlate with plaque rupture location but are also predictive of where the rupture will occur [18, 19]. While these studies are illuminating and informative, they remain computational models in need of corroboration from direct measurements of strain.

Intravenous ultrasound (IVUS) provides the best evidence that strain mapping of the carotid arteries will show great promise. IVUS utilizes cross-sectional analysis of radiofrequency ultrasound signals recorded at different intervals of the vascular cycle as shown in figure 1.2. It utilizes a probe that must be inserted into the carotid artery surgically. A study using excised artery segments showed that circumferential strain provides 88% sensitivity and 89% specificity for detection of vulnerable plaques [21]. Animal studies show even more promising results with a sensitivity and specificity of 92% [22]. Furthermore, a recent study showed that strain may be predictive of plaque formation [23]. While these results show that strain mapping will be valuable in the diagnosis of atherosclerosis, IVUS suffers from several drawbacks. First, it is not widely available and requires highly skilled training. Second, it suffers from reproducibility issues based on catheter position [24]. Finally, and most importantly, it is an invasive technique that carries with it inherent dangers to the patient. A noninvasive technique

such as MRI could overcome the danger as well as difficulties with availability and reproducibility.

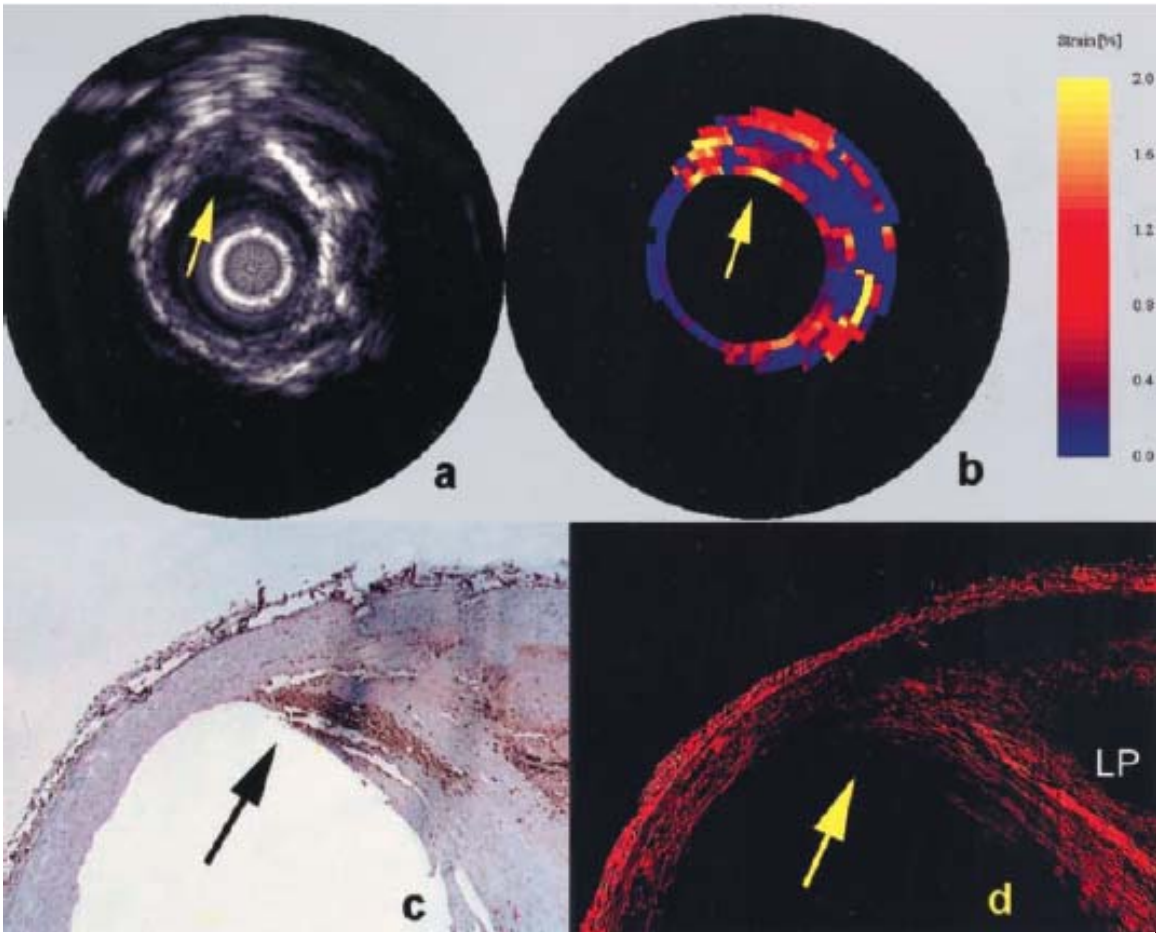

Figure 1.2 IVUS of vulnerable plaque. A) IVUS image where the yellow arrow indicates the vulnerable plaque B) Elastogram of color-coded circumferential strain. The area of vulnerable plaque shows high strain on the surface. C) Macrophage-stained histology corroborating area of vulnerable plaque. D) Collagen stained histology showing the lipid pool (LP). From reference [21].

Three noninvasive MRI techniques are now available which can be used to track various time points in the cardiac cycle. These are tagging [25, 26], phase contrast [27, 28], and DENSE [29]. Tagging utilizes spatial saturation bands that when placed as a grid can be used to measure displacement of tissue. This method suffers from signal loss at the end of the cardiac cycle and is limited by the resolution of the saturation bands. Phase contrast imaging utilizes the change in phase to map displacement, but it has been

primarily used for blood flow measurements and does not have sufficient SNR for strain measurements. The DENSE method takes advantage of the stimulated echo which maintains phase information in the longitudinal direction that does not decay as quickly as in the transverse plane. The encoding and decoding gradient pulses are separated by the mixing time (TM), so that spin displacement during this time causes a phase shift in the acquired image which is proportional to the net displacement in the direction of the gradient. From this displacement, cyclic or circumferential strain can be calculated. This method has been utilized for cardiac studies where circumferential strain from DENSE-MRI has been shown to be effective for diagnosing abnormal wall motion [30] and can not only help to define infracted tissue [31] but also the area at risk for reperfused acute myocardial infarction which has key implications for intervention and treatment of heart attacks [32]. However, none of the displacement-encoded MRI methods has been applied in the carotid arteries.

Goals

The goals of this study are to develop a noninvasive, quantitative method of measuring strain the carotid arteries and to utilize this method to characterize strain patterns in atherosclerosis. This will be achieved by

1. Adapting DENSE-MRI to the carotid arteries using a segmented pulse sequence with a steady state free precession readout that achieves the highest signal-to-noise ratio (SNR) in order to provide the resolution necessary for the carotid arteries.
2. Validating the strain measurements by comparing the average circumferential strain as measured by DENSE-MRI with the change in systolic to diastolic lumen

area as measured by CINE MRI at both 1.5T and 3.0T field strengths. If successful, a high correlation between this global measure of strain is expected.

3. Improving the DENSE-MRI sequence by utilizing a single-shot pulse sequence that will eliminate artifacts due to irregular in-plane flow and subject motion.
4. Measuring strain in the common carotid artery at different levels of plaque buildup. This will be achieved by acquiring strain measurements in human subjects at various ages which should show increasing carotid lumen wall thickness with age and where it is expected that strain will decrease.
5. Measure strain in subjects that have had strokes and compare the strain values with healthy age-matched controls. If strain is diagnostic, a significant difference between the patients and controls should emerge.

The result of this study will be a novel, robust, direct measurement of carotid artery wall stiffness using a nonsurgical alternative to current medical technologies. Given the strong correlation between stiffness and the formation of atherosclerotic plaques, future studies based on our findings could be conducted in multicenter trials to determine if DENSE-MRI is predictive for potential stroke. The pulse sequence would be readily available at clinical centers across the world where much of the underlying technology already exists. In addition to providing important diagnostic information, this test can also be used to monitor treatment in patients to determine the efficacy of pharmaceutical treatments such as the popular statin medications. Most importantly, DENSE-MRI provides a noninvasive measure of properties that underlie the greatest health problem our society faces today.

Organization

Upon the completion of this study, the full translation of a method from benchtop concepts of biomechanics to the potential bedside application as a diagnostic tool will be shown. As such, the organization of the thesis is intentional and intends to demonstrate the development of these methods at each step. This thesis is based on peer-review articles from archival journals spanning technical development to clinical results. The thesis author is the lead author of all articles and wrote all or a large majority of them.

The second chapter describes the validation of the DENSE-MRI technique in the carotid arteries at 1.5T and 3.0T [33, 34]. To our knowledge, this is the first demonstration of strain mapping of the carotid arteries using MRI. It is important to note that while global measures of strain by determining circumferential changes in lumen diameter are readily available, the mapping of strain at individual points across the lumen has never been achieved at the resolution provided by DENSE-MRI.

Validation of DENSE-MRI was conducted at the common carotid artery where global measures of strain were possible. It is of greater interest to examine strain at the bifurcation and in the internal and external carotid arteries where traditional methods of measuring strain are not possible due to the complex geometry at those points. However, segmented DENSE-MRI suffered from imaging artifacts at the bifurcation and above. In order to surmount this problem, a single-shot DENSE-MRI sequence was developed and tested [35, 36]. Chapter 3 describes this sequence in detail as well as improvements in the data postprocessing that also helped to eliminate artifacts from subject motion. The material in this chapter was expanded from the original submitted manuscript by

including *in vitro* studies where models of the carotid arteries were developed to test the pulse sequence during development. The ultimate test of success however is shown, as in the manuscript, by quantifying the improvements of single-shot sequence over the segmented sequence in human subjects at both 1.5T and 3.0T.

With these methods validated and optimized, the next step in translational research is to apply these methods in a normal population. The fourth chapter describes the results of DENSE measurements in a cohort of healthy subjects. Strain is characterized across a range of ages and subsequent lumen wall thickness. Furthermore, a small cohort of patients with a history of stroke were also examined and their results compared to the healthy cohort. This chapter provides the framework for future studies that establish the clinical relevance of DENSE-MRI.

A case study of a patient where DENSE-MRI was acquired in known atherosclerosis corroborated by ultrasound and CT scans is presented in the fifth chapter. This case illustrates many of the results observed in the fourth chapter and demonstrates the added value of DENSE-MRI carotid strain maps in a clinical environment.

Finally, the thesis concludes with limitations of the studies and future research that would help to better define the efficacy of carotid DENSE-MRI.

References

1. Rosamond, W., Flegal, K., Friday, G., Furie, K., Go, A., Greenlund, K., Haase, N., Ho, M., Howard, V., Kissela, B., et al., Heart disease and stroke statistics--2007 update: a report from the American Heart Association Statistics Committee and Stroke Statistics Subcommittee. *Circulation* **2007,** 115(5), e69–171.
2. Atherosclerosis. *Heart and Stroke Encyclopedia.* Available from http://www.americanheart.org/presenter.jhtml?identifier=4440 (Cited June 20 2007)
3. Naghavi, M., Libby, P., Falk, E., Casscells, S. W., Litovsky, S., Rumberger, J., Badimon, J. J., Stefanadis, C., Moreno, P., Pasterkamp, G., et al., From vulnerable plaque to vulnerable patient: a call for new definitions and risk assessment strategies: Part I. *Circulation* **2003,** 108(14), 1664–1672.
4. Ali, M. H., Pearlstein, D. P., Mathieu, C. E., Schumacker, P. T., Mitochondrial requirement for endothelial responses to cyclic strain: implications for mechanotransduction. *Am J Physiol Lung Cell Mol Physiol* **2004,** 287(3), L486–496.
5. Cheng, J. J., Chao, Y. J., Wang, D. L., Cyclic strain activates redox-sensitive proline-rich tyrosine kinase 2 (PYK2) in endothelial cells. *J Biol Chem* **2002,** 277(50), 48152–48157.
6. Cheng, J. J., Wung, B. S., Chao, Y. J., Hsieh, H. J., Wang, D. L., Cyclic strain induces redox changes in endothelial cells. *Chin J Physiol* **1999,** 42(2), 103–111.
7. Cheng, J. J., Wung, B. S., Chao, Y. J., Wang, D. L., Cyclic strain-induced reactive oxygen species involved in ICAM-1 gene induction in endothelial cells. *Hypertension* **1998,** 31(1), 125–130.

8. Lehoux, S., Esposito, B., Merval, R., Loufrani, L., Tedgui, A., Pulsatile stretch-induced extracellular signal-regulated kinase 1/2 activation in organ culture of rabbit aorta involves reactive oxygen species. *Arterioscler Thromb Vasc Biol* **2000,** 20(11), 2366–2372.

9. Tummala, P. E., Chen, X. L., Medford, R. M., NF- kappa B independent suppression of endothelial vascular cell adhesion molecule-1 and intercellular adhesion molecule-1 gene expression by inhibition of flavin binding proteins and superoxide production. *J Mol Cell Cardiol* **2000,** 32(8), 1499–1508.

10. Lusis, A. J., Atherosclerosis. *Nature* **2000,** 407(6801), 233-41.

11. Cheng, J. J., Wung, B. S., Chao, Y. J., Wang, D. L., Cyclic strain enhances adhesion of monocytes to endothelial cells by increasing intercellular adhesion molecule-1 expression. *Hypertension* **1996,** 28(3), 386–391.

12. Cheng, G. C., Briggs, W. H., Gerson, D. S., Libby, P., Grodzinsky, A. J., Gray, M. L., Lee, R. T., Mechanical strain tightly controls fibroblast growth factor-2 release from cultured human vascular smooth muscle cells. *Circ Res* **1997,** 80(1), 28–36.

13. Clowes, A. W., Reidy, M. A., Clowes, M. M., Mechanisms of stenosis after arterial injury. *Lab Invest* **1983,** 49(2), 208–215.

14. DeBakey, M. E., Lawrie, G. M., Glaeser, D. H., Patterns of atherosclerosis and their surgical significance. *Ann Surg* **1985,** 201(2), 115–131.

15. Thubrikar, M. J., Robicsek, F., Pressure-induced arterial wall stress and atherosclerosis. *Ann Thorac Surg* **1995,** 59(6), 1594–1603.

16. Baldewsing, R. A., Schaar, J. A., Mastik, F., Oomens, C. W., van der Steen, A. F., Assessment of vulnerable plaque composition by matching the deformation of a

parametric plaque model to measured plaque deformation. *IEEE Trans Med Imaging* **2005,** 24(4), 514–528.

17. Lee, R. T., Loree, H. M., Cheng, G. C., Lieberman, E. H., Jaramillo, N., Schoen, F. J., Computational structural analysis based on intravascular ultrasound imaging before in vitro angioplasty: prediction of plaque fracture locations. *J Am Coll Cardiol* **1993,** 21(3), 777–782.

18. Ohayon, J., Teppaz, P., Finet, G., Rioufol, G., In-vivo prediction of human coronary plaque rupture location using intravascular ultrasound and the finite element method. *Coron Artery Dis* **2001,** 12(8), 655–663.

19. Li, Z. Y., Howarth, S., Trivedi, R. A., JM, U. K.-I., Graves, M. J., Brown, A., Wang, L., Gillard, J. H., Stress analysis of carotid plaque rupture based on in vivo high resolution MRI. *J Biomech* **2006,** 39(14), 2611–2622.

20. Younis, H. F., Kaazempur-Mofrad, M. R., Chan, R. C., Isasi, A. G., Hinton, D. P., Chau, A. H., Kim, L. A., Kamm, R. D., Hemodynamics and wall mechanics in human carotid bifurcation and its consequences for atherogenesis: investigation of inter-individual variation. *Biomech Model Mechanobiol* **2004,** 3(1), 17–32.

21. Schaar, J. A., De Korte, C. L., Mastik, F., Strijder, C., Pasterkamp, G., Boersma, E., Serruys, P. W., Van Der Steen, A. F., Characterizing vulnerable plaque features with intravascular elastography. *Circulation* **2003,** 108(21), 2636–2641.

22. de Korte, C. L., Sierevogel, M. J., Mastik, F., Strijder, C., Schaar, J. A., Velema, E., Pasterkamp, G., Serruys, P. W., van der Steen, A. F., Identification of atherosclerotic plaque components with intravascular ultrasound elastography in vivo: a Yucatan pig study. *Circulation* **2002,** 105(14), 1627–1630.

23. Schmitt, C., Soulez, G., Maurice, R. L., Giroux, M. F., Cloutier, G., Noninvasive vascular elastography: toward a complementary characterization tool of atherosclerosis in carotid arteries. *Ultrasound Med Biol* **2007,** 33(12), 1841–1858.

24. De Korte, C. L., Cespedes, E. I., Van Der Steen, A. W., Influence of catheter position on estimated strain in intravascular elastography. *IEEE Trans Ultrason Ferroelectr Freq Control* **1999,** 46(3), 616–625.

25. Axel, L., Dougherty, L., MR imaging of motion with spatial modulation of magnetization. *Radiology* **1989,** 171(3), 841–845.

26. Zerhouni, E. A., Parish, D. M., Rogers, W. J., Yang, A., Shapiro, E. P., Human heart: tagging with MR imaging--a method for noninvasive assessment of myocardial motion. *Radiology* **1988,** 169(1), 59–63.

27. Bryant, D. J., Payne, J. A., Firmin, D. N., Longmore, D. B., Measurement of flow with NMR imaging using a gradient pulse and phase difference technique. *J Comput Assist Tomogr* **1984,** 8(4), 588–593.

28. Pelc, N. J., Drangova, M., Pelc, L. R., Zhu, Y., Noll, D. C., Bowman, B. S., Herfkens, R. J., Tracking of cyclic motion with phase-contrast cine MR velocity data. *J Magn Reson Imaging* **1995,** 5(3), 339–345.

29. Aletras, A. H., Ding, S., Balaban, R. S., Wen, H., DENSE: displacement encoding with stimulated echoes in cardiac functional MRI. *J Magn Reson* **1999,** 137(1), 247–252.

30. Wen, H., Marsolo, K. A., Bennett, E. E., Kutten, K. S., Lewis, R. P., Lipps, D. B., Epstein, N. D., Plehn, J. F., Croisille, P., Adaptive postprocessing techniques for myocardial tissue tracking with displacement-encoded MR imaging. *Radiology* **2008,** 246(1), 229–240.

31. Ashikaga, H., Mickelsen, S. R., Ennis, D. B., Rodriguez, I., Kellman, P., Wen, H., McVeigh, E. R., Electromechanical analysis of infarct border zone in chronic myocardial infarction. *Am J Physiol Heart Circ Physiol* **2005,** 289(3), H1099–1105.

32. Aletras, A. H., Tilak, G. S., Natanzon, A., Hsu, L. Y., Gonzalez, F. M., Hoyt, R. F., Jr., Arai, A. E., Retrospective determination of the area at risk for reperfused acute myocardial infarction with T2-weighted cardiac magnetic resonance imaging: histopathological and displacement encoding with stimulated echoes (DENSE) functional validations. *Circulation* **2006,** 113(15), 1865–1870.

33. Lin, A. P., Bennett, E., Wisk, L., Gharib, M., Fraser, S., Wen, H., Circumferential strain in the wall of the common carotid artery: Comparing displacement-Encoded and CINE MRI in volunteers. *Magn Reson Med* **2008,** 60(1), 8–13.

34. Lin, A. P., Tyszka, J. M., Bennett, E., Fraser, S., Wen, H., Preliminary validation of circumferential strain measurements using DENSE at 1.5T and 3T. *J Cardiovasc Magn Reson* **2006,** 8(1), 48–49.

35. Lin, A. P., Bennett, E., Le, Y., Fraser, S., Wen, H. Single-shot DENSE MRI of the carotid arteries, in Proceedings of International Society of Magnetic Resonance in Medicine, Toronto, Canada, 2008; Toronto, Canada, 2008.

36. Lin, A. P., Bennett, E., Wisk, L., Gharib, M., Fraser, S., Wen, H. Mapping 2D strain in the wall of the carotid artery using displacement-encoded MRI., in Proceedings of International Society of Magnetic Resonance in Medicine, Berlin, Germany, 2007; Berlin, Germany, 2007.

Chapter 2: DENSE Strain Validation

Abstract

The wall of conduit arteries undergoes cyclic stretching from the periodic fluctuation of the arterial pressure. Atherosclerotic lesions have been shown to localize to regions of excessive stretching of the arterial wall. We employed a displacement-encoded MRI (DENSE) sequence to image the motion of the common carotid artery wall and map the 2D circumferential strain. The sequence utilizes a fully-balanced SSFP readout with 0.60 mm in-plane resolution. Preliminary results in volunteers at 1.5T (N = 4) and 3.0T (N = 17) are compared to measurements of the lumen circumference from CINE images. The agreement between the two independent measurements at both field strengths ($p \leq 0.001$) supports the use of DENSE as a means to map the pulsatile strain in the carotid artery wall.

Introduction

Stroke is the leading cause of serious, long-term disability and the third leading cause of death in the United States [1]. Strokes occur when atherosclerotic plaques grow large enough to block the flow of blood through the vessel (stenosis) or rupture, causing blood clots (thrombosis) to form in the arteries that supply blood and oxygen to the brain [2].

Changes of arterial wall strain pattern may be associated with this process in several ways. First, the arterial wall may harden or stiffen due to atherosclerotic plaque

formation [3]. The hardening of the wall leads to a reduction of the pressure-driven cyclic stretching, or strain, which lends itself to characterization by displacement-based strain mapping; excessive stretching at branching and curved locations of the arterial tree may also be a relevant mechanical factor in the development of atherosclerosis [4]. This is empirically supported by surgical evidence that the distribution of atherosclerotic plaques predominates at bifurcation points, such as the carotid arteries [5]; once the plaques are formed, 70% of them tend to rupture [6]. The rupture event may also be related to mechanical weakening and excessive strain in the plaque under arterial pressure loading. Evidence to support this connection has been shown with intravenous ultrasound (IVUS) in excised atherosclerotic coronary segments under pulsatile pressure loading [7]. The IVUS measurements show increased strain that extends indepth beneath the thin cap of the plaques that rupture. *In vivo* IVUS studies of the culprit segment in patients with acute coronary syndrome also showed a clear separation of low vs. high strain in patients with stable symptoms vs. those with unstable chest pain or postmyocardial infarction [8]. For these reasons, noninvasive imaging of the arterial wall strain pattern may provide additional information on the risk of atherosclerosis and the classification of plaques.

Further evidence that strain in the carotid wall may be relevant to atherogenesis come from finite element analysis generated from IVUS [9-11] and MRI [12, 13] images. The results of these studies show that high strain can be found at regions of the carotid bifurcation that correlate with sites of early atherosclerotic inflammation [13]. Focal regions of high strain in the fibrous cap not only correlate with plaque rupture location but are also predictive of where the rupture will occur [11, 12]. While these studies are illuminating and informative, they remain computational models in need of corroboration from direct measurements of strain.

The only means for mapping strain in the arterial wall that we are aware of is intravascular ultrasound, an invasive technique. We adapted a displacement encoding with stimulated echoes (DENSE) [14-16] pulse sequence to measure the 2D displacement vectors of the carotid artery wall and the surrounding tissue and calculated circumferential strain distribution. DENSE has been primarily used to track motion of the myocardial wall and more recently brain tissue [17], producing color-coded strain maps that represents active contraction or passive deformation. The purpose of this study is to test its ability to map the carotid wall strain distribution [18] and validate the results in normal volunteers at 1.5T and 3.0T against measurements of lumen circumference from CINE scans.

Methods

The DENSE sequence with balanced SSFP, or true-FISP readout is illustrated in figure 2.1. The DENSE method takes advantage of the stimulated echo which maintains phase information in the longitudinal direction that does not decay as quickly as in the transverse plane. The encoding and decoding gradient pulses are separated by the mixing time TM, so that spin displacement during this time causes a phase shift in the acquired image which is proportional to the net displacement in the direction of the gradient. A detailed explanation of this idea is given in several references [16, 19]. One benefit of using stimulated echoes at long TM periods is that it provides inherent black-blood contrast in the images. This is due to rapid motion of blood during the displacement-encoding period that results in severe intravoxel dephasing and signal loss, thus providing inherent contrast between the vessel wall and blood flow. In the application of DENSE to

the carotid artery we need to achieve sufficient signal level at a relatively high spatial resolution in the carotid wall, and opted for the balanced SSFP readout [20-22].

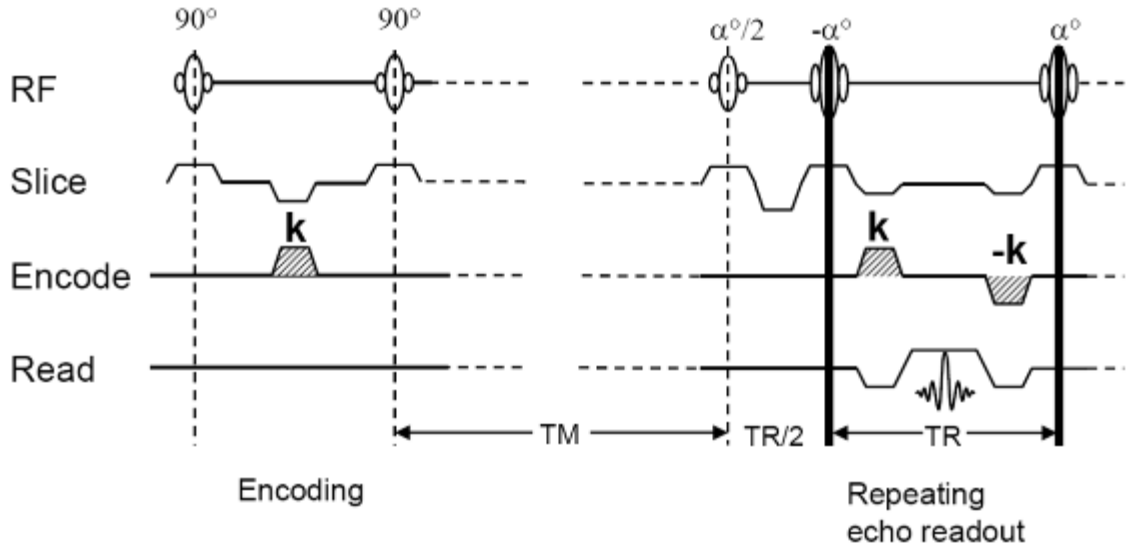

Figure 2.1 Illustration of the DENSE with balanced-SSFP readout pulse sequence. The gradient pulse **k** encodes spin displacement into a phase shift of the image. TR is the repetition time of the readout, and TM is the mixing time allowing spin displacement to occur.

Referring to figure 2.1, the displacement-encoding section is followed by a train of true-FISP readout segments, each acquiring a k-space line. The flip angles of the train are ramped to equalize the signal amplitudes [20, 22]. It is important to note that true-FISP sequences are more dependent on B0 uniformity. Additional shimming, especially at 3.0T where B0 susceptibility is more pronounced, is necessary as described below. Signal averaging in the form of phase cycling was used to improve SNR and remove the unwanted FID and stimulated-anti-echo signals [23-25].

Normal volunteer scans were performed at 1.5T (n = 4, all male, age 29 to 37) using a 4 channel carotid coil pair (MachNet, Netherlands), and at 3T (n = 17, 7 males. 10 females, age 18 to 66) using a surface coil (NOVA, Boston, MA). Scans were conducted under IRB approved volunteer protocols (NHLBI MRI Technical Development Protocol for 1.5T and Caltech SF-88 for 3T) and informed consent was

obtained. The same scan parameters were used at both field strengths. Initial three plane scout images were acquired to localize of the left and/or right carotid artery and optimize coil location. Two dimensional TOF images were acquired and MIPs used for slice positioning. Three slices were positioned at the common carotid artery such that the superior slice was placed 10 mm below the bifurcation point. An ECG-gated CINE scan was acquired at the same location and resolution as DENSE images to determine the time points of maximum and minimum lumen diameter. DENSE images were acquired using a matrix size of 256 * 192 to provide a resolution of 0.60 * 0.60 * 4mm. A bandwidth of 585 Hz per pixel was used with a true-FISP readout of 32 k-space lines per heartbeat, and TR/TE = 4.8/2.4 ms. Signal averaging, or phase cycling, of 10 was used. Displacement encoding was acquired in three oblique directions ([0, 1, 1], [0, -1, 1], [1, 0, 1]) to produced a pixel-by-pixel 2D displacement map. In DENSE measurements, the number of phase maps with independent displacement encoding directions is one more than the desired displacement components, so that one phase map serves as a reference map which is subtracted from the other two encoding maps to remove phase errors associated with B0 field homogeneity and other sources of phase variation [14, 24]. The encoding gradient area was 0.60 π/mm inplane. The scans were triggered by the R-wave of the ECG, and image acquisition was consistently placed at the time of maximum lumen diameter judging from the CINE scans, while in two separate scans the encoding portion was placed at 40 ms and 80 ms after the R-wave to capture the maximum wall strain and intermediate strain (figure 2.2). At 1.5T, 3 slices were acquired from both the left and right carotid arteries at maximum strain and at intermediate strain which resulted in a total of 51 DENSE strain measurements in the 4 volunteers. At 3.0T, the single surface coil had a limited FOV and only allowed a single side of the neck to be scanned, resulting

in a single slice acquired separately at maximum and intermediate strain for a total of 34 strain data points in the 17 volunteers. The total scan time for a slice was 6 minutes. Total protocol scan time was less than 45 minutes. Vacuum fixation cushions (VacFix, PAR Scientific, Denmark) were utilized to minimize movement effects due to swallowing.

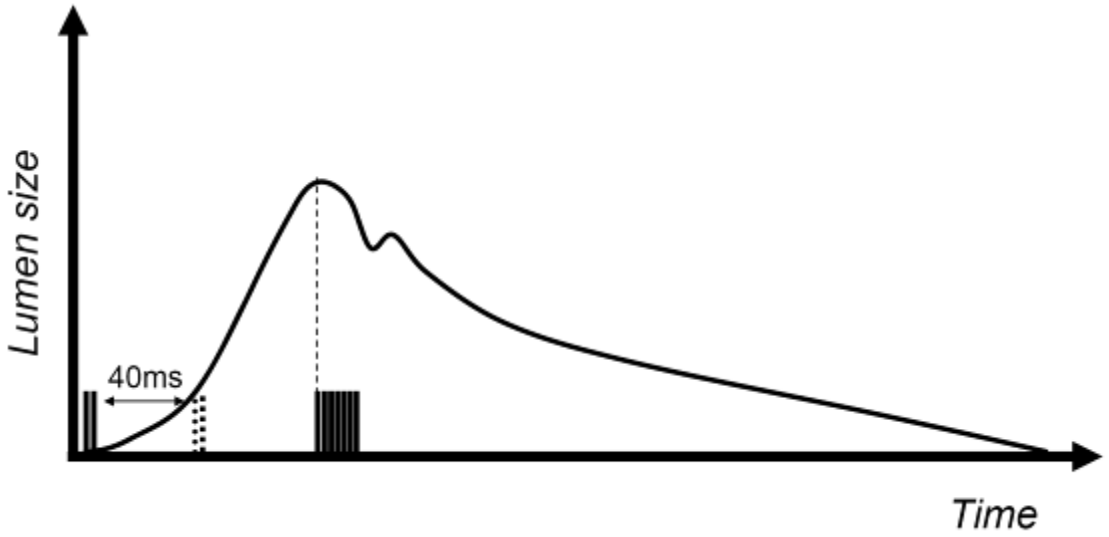

Figure 2.2. DENSE pulse sequence timing shown with lumen diameter changes from systole to diastole. The scans were triggered by the R-wave of the ECG, and image acquisition was consistently placed at the time of maximum lumen diameter judging from the CINE scans, while in two separate scans the encoding portion was placed at 40 and 80 ms (dotted) after the R-wave to capture the maximum wall strain and intermediate strain. The readout remains the same in both scans.

While the 1.5T scans were relatively routine, imaging at 3.0T introduced technical issues such as the lack of FDA-approved dual surface coils, increased sensitivity to off-resonance effects from the true-FISP readout, and increased artifacts in the ECG signal. These obstructions were surmounted by optimizing coil placement, manual setting of the shim volume, and centralized lead placement, respectively. Manual shim volume setting was completed by using localized shim volumes surrounding the scanned region and applying automated shimming which was often repeated twice to achieve optimal shim.

For postprocessing, DENSE-MRI strain measurements were calculated taking all quadrilateral elements of neighboring pixels. The circumferential strain (Ecc) is a projection of the Lagrangian strain tensor [26]

$$S = \frac{1}{2}(E^T E - 1), \tag{2.1}$$

where E is the tissue deformation matrix from the in-plane displacement (Dx, Dy) of each quadrilateral element:

$$E = \begin{pmatrix} \frac{\partial D_x}{\partial x} & \frac{\partial D_x}{\partial y} \\ \frac{\partial D_y}{\partial x} & \frac{\partial D_y}{\partial y} \end{pmatrix}. \tag{2.2}$$

The elements of the matrix are calculated from linear regression of the displacement vectors relative to the coordinates of the pixels in the image. The circumferential strain is the projection of the strain tensor onto the circumferential direction ec:

$$E_{cc} = \boldsymbol{e}_c^{\,T} S \boldsymbol{e}_c. \tag{2.3}$$

The ec direction is based on a manually drawn contour of the vessel wall. Once the Ecc strain map is obtained, the mean Ecc strain value around the lumen, or <Ecc>, is calculated as the average of the pixel values over the contour as shown in figure 2.3. The variance of the strain value around the lumen was also obtained. These measurements are semiautomated using software (DENSEview) written for DENSE strain measurements.

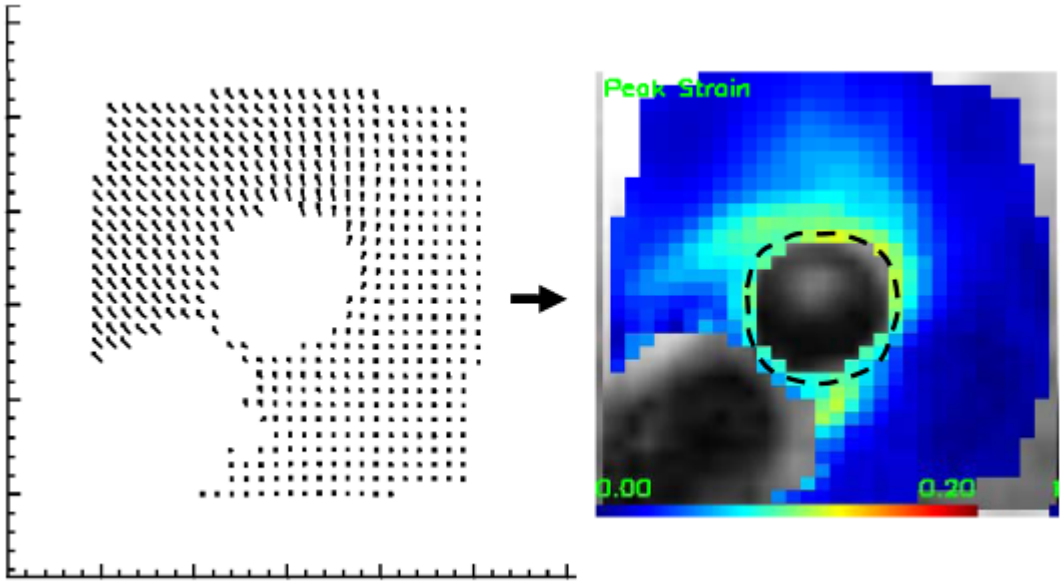

Figure 2.3. DENSE strain measurements. Left: Displacement map generated from the phase images acquired at 1.5T. Right: E_{cc} strain map that is derived from the displacement vectors as described in the "method" section. Dotted line indicates the contour from which average strain is calculated.

For comparison with an independent measurement, we note that the mean circumferential strain around the lumen of the artery is effectively the fractional change of its circumference, which can be measured in CINE MR images using the circumference of the lumen at the initial and end time points of the DENSE mixing time. In the CINE images the lumen boundary was drawn manually for the frames corresponding to the initial and end time points. The irregular shape of the cross-section at the bifurcation would make lumen circumference unreliable, therefore slices in the common carotid artery were used for CINE measurements. The fractional change of the circumference was then used to provide the mean <Ecc'> measurement by CINE:

$$< E_{cc}' >= \frac{(C_{end} - C_{init})}{C_{end}}.$$

To compare the mean Ecc from the DENSE <Ecc> and CINE <Ecc'> measurements, we performed correlation and Bland-Altman analysis at both field strengths between the two techniques. The correlation and Bland-Altman included all data using both peak strain

(40 ms after the R-wave) and intermediary strain (80 ms after the R-wave) measured by DENSE with corresponding strain measured from CINE. Additionally, we also measured the signal-to-noise ratio of the DENSE data in the carotid wall for 1.5T and 3T separately.

Results

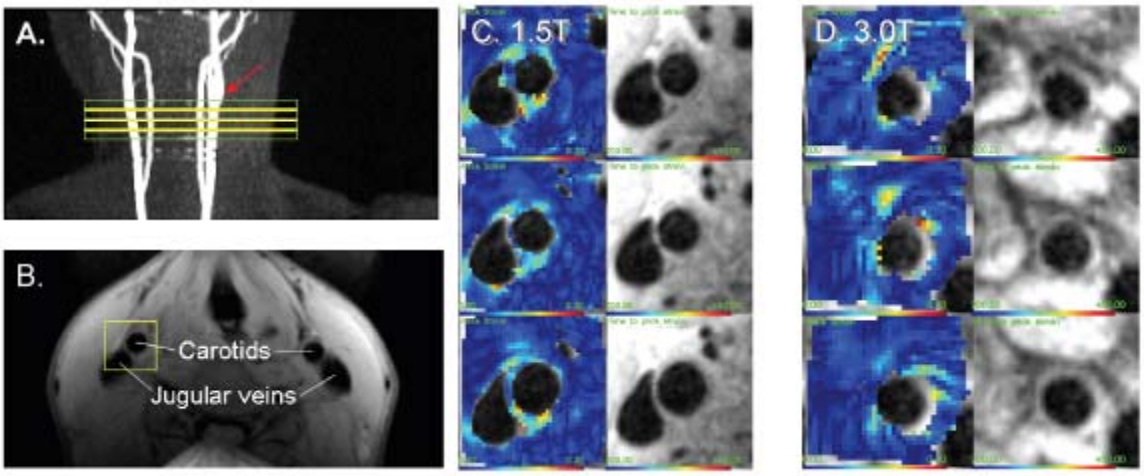

Figure 2.4. DENSE MRI. A) Slice locations (dotted lines) and shim volume (rectangle) of the DENSE and CINE MRI are indicated on maximum intensity projection images of 2D TOF MRI. Arrow indicates the carotid bifurcation used as a landmark. B) Raw DENSE phase image acquired at 1.5T. The rectangular volume indicates the area that is postprocessed using the DENSEview software. C) Three slices of the DENSE MRI acquired at 1.5T starting at the top from the inferior portion of the common carotid to just below the bifurcation. D) Three slices of the DENSE MRI acquired at 3.0T in the same order.

Figure 2.4 shows the slice location and region of strain analysis around the carotid arteries using the DENSE technique. At 1.5T the average SNR ratio of the DENSE images among the volunteers was 2.6 in the segment of the wall bordering the jugular vein, 4.6 in the opposite segment, and 3.4 over the whole circumference. Correspondingly, the pixel-wise displacement noise was between 44 and 78 μm, and the pixel-wise Ecc strain noise was between 0.10 and 0.18, with an average of 0.14. At 3.0T, the average SNR ratio ranged from 1.9 in the segment furthest from the surface coil to

14.9 in the most superficial segment, and 6.3 over the circumference. The corresponding pixel-wise strain noise is between 0.032 and 0.25, with an average of 0.076. The variation of SNR matches the sensitivity profile of the single surface coil used for 3T imaging.

The average Ecc strain around the carotid circumference between diastole and systole represents the total distension of the circumference. In the 1.5T group this was 0.076 ± 0.006 (mean ± stdev) by DENSE (<Ecc>) and 0.079 ± 0.007 by CINE (<Ecc'>). In the 3T group <Ecc> was 0.072 ± 0.039 and <Ecc'> was 0.071 ± 0.031. The two groups consisted of different volunteers, and as a result have different ranges of Ecc strain. However, they were not statistically different from each other (P=0.77). The average <Ecc> of both groups combined is 0.072 ± 0.026 by DENSE.

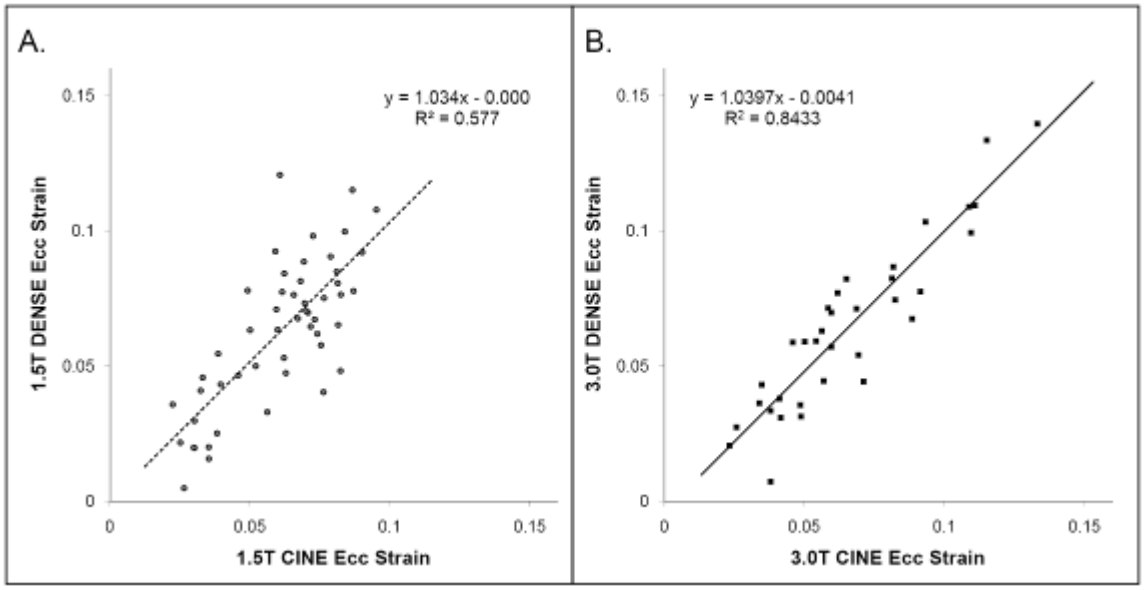

Figure 2.5. CINE and DENSE correlation at A) 1.5T and B) 3.0T. The results of the least squares linear fit are shown for both field strengths.

The correlation between DENSE <Ecc> and CINE <Ecc'> measurements show good agreement (Figure 2.5). The mean and 95% confidence level of the correlation coefficient are 1.03 and 0.78 to 1.29 at 1.5T (R2 = 0.58), and 1.03 and 0.88 to 1.20 at 3T

($r^2 = 0.84$). Paired t-tests between CINE and DENSE values show no statistical difference between the two at both 1.5T and 3T ($p = 0.45$ and 0.50, respectively).

The Bland-Altman analysis (Figure 2.6) indicates that the variance of the difference between DENSE <Ecc> and CINE <Ecc'> is 0.035 at 1.5T and 0.025 at 3T. The mean of the difference between these two methods is 0.002 at 1.5T and -0.001 at 3T. The latter represent systematic biases of DENSE relative to CINE, and are statistically not significant at either field strength ($p = 0.45$ and 0.50 respectively).

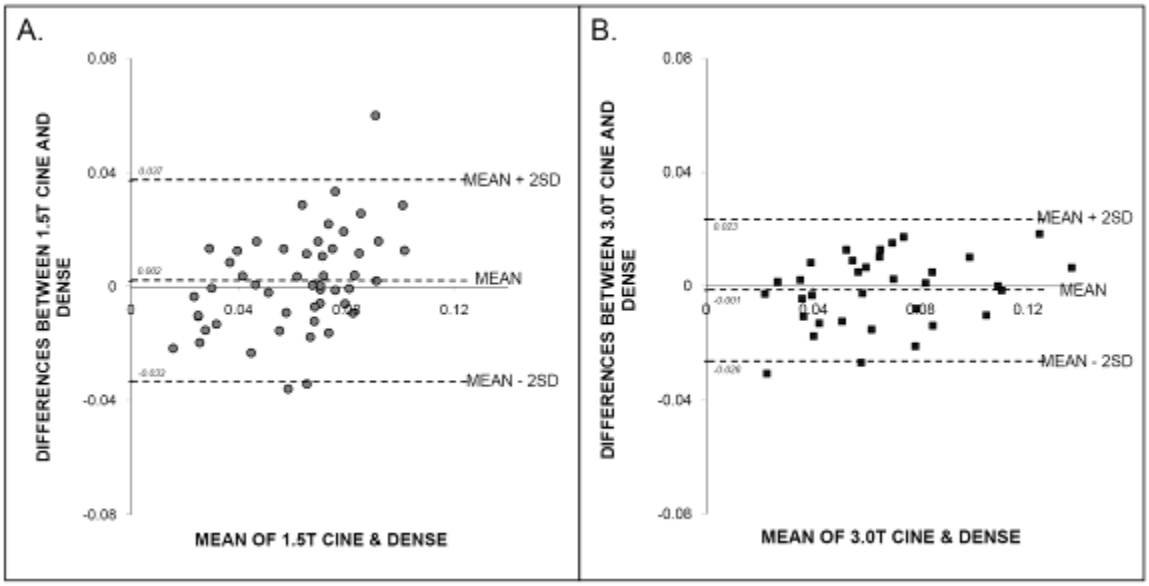

Figure 2.6. Bland-Altman graphs at A) 1.5T and B) 3.0T. The Bland-Altman graphs compare difference between the DENSE and CINE strain measurements plotted against the mean of the two measurements. Mean ± two standard deviations are indicated by the dotted lines to show the 95% confidence interval.

It is important to note that DENSE provides Ecc on a pixel-wise basis, a regional measures of strain which is different from the global mean <Ecc'> made from CINE measurements. Since currently there does not exist an equivalent noninvasive measurement of regional strain, it is informative to investigate the spatial variation of the strains measured. Figure 2.7 plots the variance of strain around the lumen circumference vs. the mean strain level. The results show that variance increases linearly with the mean

strain. This indicates that there exists a spatial heterogeneity of strain which scales with the mean strain and contributes to the measured variance, in addition to any random noise that is independent from the mean strain. In the 1.5T group, the amplitude of the spatial variance is 50% of mean strain, whereas in the 3.0T group, it is 35% of the mean strain. This difference may be due to the different age ranges of the two groups and warrants further study.

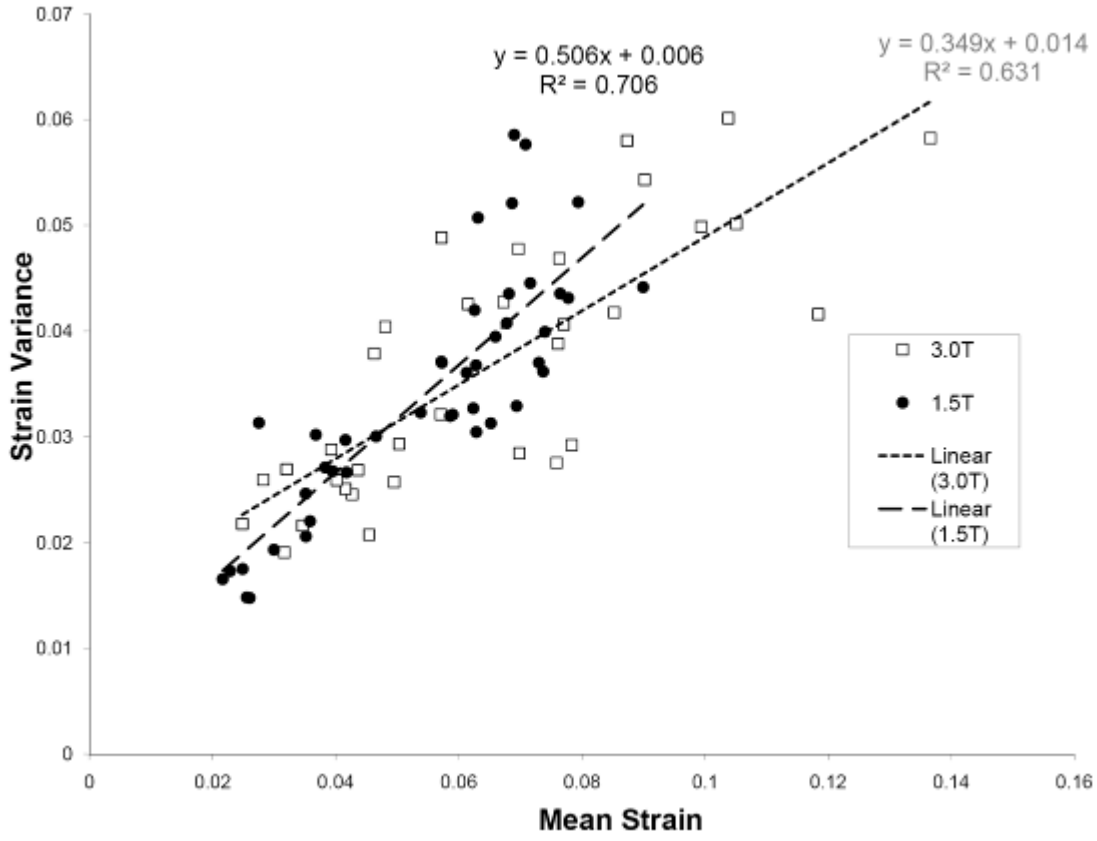

Figure 2.7. Spatial variance of strain at 1.5T and 3.0T. The DENSE strain variance around the lumen wall is correlated linearly with the mean DENSE strain measurements, indicating a real spatial heterogeneity in addition to random noise variation.

Discussion

The results of the correlation analysis demonstrate that there is good agreement between DENSE strain and CINE lumen size measurements at both 1.5T and 3.0T. The Bland-

Altman plots show that the variability of DENSE values relative to CINE is lower at 3.0T than at 1.5T. The increased SNR at 3.0T is the likely reason for the lower variability. Previous studies have shown that direct lumen measurements from CINE MRI show excellent agreement with lumen wall distention measurements using ultrasound [27, 28]. Crowe and coauthors measured the area distension of the common carotid lumen between diastole and systole in a group of volunteers using CINE MRI and found it to be 15.1% ± 5.1%. This translates to a circumferential distension of 0.072 ± 0.021, which is in good agreement with our result of 0.072 ± 0.026. Using similar calculations from lumen area and/or diameter, other studies show a range of circumferential distension in normal subjects using MRI (0.103 [28], 0.152 [29]) or ultrasound (0.052 [30], 0.056 [30], 0.086 [28], 0.088 [27]) of which our DENSE results are within the range.

Theoretically, there is an expected two times signal gain when moving from 1.5T to 3T. However, the SNR comparisons at both fields show that while there is SNR gain in the segment closest to the surface coil, there is also signal loss in the distal segment due to the sensitivity profile of the single surface coil used at 3T. We also observed that the signal drop off was greatly influenced by the wide range of the subject's neck geometries. The surface coil was the only commercially available coil approved for 3T use at the time of this study. Future array coils for neck imaging at 3T should rectify these shortcomings as will be described in chapter 3. Currently the resolution of the images is 0.6 mm inplane at 4 mm slice thickness. To improve the spatial resolution will require a trade-off of SNR or scan time. The SNR increase at 3T compared to 1.5T implies that this limitation should be eased by the use of array coils at 3T. This will allow for higher resolution images for future studies in patients with known atherosclerosis.

It should be noted that DENSE strain measurements are localized, such that regional strain differences can be measured as opposed to CINE or ultrasound lumen measurements, which provide global strain and by inference the average stiffness. While the average carotid arterial wall stiffness has been implicated in a broad range of neurological and cardiovascular diseases including stroke [31], hypertension [32], myocardial infarction [3], inflammatory disease [33], and cognitive impairment [34], regional measurement may improve the specificity and sensitivity of this test similar to what has been shown in strain mapping with intravascular ultrasound (IVUS) [8].

This preliminary study provides the groundwork from which future studies will compare regional strain values to a reference standard. Current IVUS strain mapping only provide radial strain but not circumferential distension, and cannot yet be compared with the DENSE technique. Similarly, a recent study using transcutaneous US [35] could measure circumferential strain only in some segments and was not quantified for in vivo studies, making it difficult to provide a direct comparison to DENSE. The rapid development of IVUS, ultrasound, and optical tomography imaging may soon provide an independent imaging technique as a reference standard.

References

1. Rosamond, W., Flegal, K., Friday, G., Furie, K., Go, A., Greenlund, K., Haase, N., Ho, M., Howard, V., Kissela, B., et al., Heart disease and stroke statistics--2007 update: a report from the American Heart Association Statistics Committee and Stroke Statistics Subcommittee. *Circulation* **2007,** 115(5), e69–171.
2. Atherosclerosis. *Heart and Stroke Encyclopedia.* Available from http://www.americanheart.org/presenter.jhtml?identifier=4440 (Cited June 20 2007)
3. Van Popele, N. M., Grobbee, D. E., Bots, M. L., Asmar, R., Topouchian, J., Reneman, R. S., Hoeks, A. P., van der Kuip, D. A., Hofman, A., Witteman, J. C., Association between arterial stiffness and atherosclerosis: the Rotterdam Study. *Stroke* **2001,** 32(2), 454–460.
4. Thubrikar, M. J., Robicsek, F., Pressure-induced arterial wall stress and atherosclerosis. *Ann Thorac Surg* **1995,** 59(6), 1594–1603.
5. DeBakey, M. E., Lawrie, G. M., Glaeser, D. H., Patterns of atherosclerosis and their surgical significance. *Ann Surg* **1985,** 201(2), 115–131.
6. Naghavi, M., Libby, P., Falk, E., Casscells, S. W., Litovsky, S., Rumberger, J., Badimon, J. J., Stefanadis, C., Moreno, P., Pasterkamp, G., et al., From vulnerable plaque to vulnerable patient: a call for new definitions and risk assessment strategies: Part I. *Circulation* **2003,** 108(14), 1664–1672.
7. Schaar, J. A., De Korte, C. L., Mastik, F., Strijder, C., Pasterkamp, G., Boersma, E., Serruys, P. W., Van Der Steen, A. F., Characterizing vulnerable plaque features with intravascular elastography. *Circulation* **2003,** 108(21), 2636–2641.

8. Schaar, J. A., Regar, E., Mastik, F., McFadden, E. P., Saia, F., Disco, C., de Korte, C. L., de Feyter, P. J., van der Steen, A. F., Serruys, P. W., Incidence of high-strain patterns in human coronary arteries: assessment with three-dimensional intravascular palpography and correlation with clinical presentation. *Circulation* **2004,** 109(22), 2716–2719.

9. Baldewsing, R. A., Schaar, J. A., Mastik, F., Oomens, C. W., van der Steen, A. F., Assessment of vulnerable plaque composition by matching the deformation of a parametric plaque model to measured plaque deformation. *IEEE Trans Med Imaging* **2005,** 24(4), 514–528.

10. Lee, R. T., Loree, H. M., Cheng, G. C., Lieberman, E. H., Jaramillo, N., Schoen, F. J., Computational structural analysis based on intravascular ultrasound imaging before in vitro angioplasty: prediction of plaque fracture locations. *J Am Coll Cardiol* **1993,** 21(3), 777–782.

11. Ohayon, J., Teppaz, P., Finet, G., Rioufol, G., In-vivo prediction of human coronary plaque rupture location using intravascular ultrasound and the finite element method. *Coron Artery Dis* **2001,** 12(8), 655–663.

12. Li, Z. Y., Howarth, S., Trivedi, R. A., JM, U. K.-I., Graves, M. J., Brown, A., Wang, L., Gillard, J. H., Stress analysis of carotid plaque rupture based on in vivo high resolution MRI. *J Biomech* **2006,** 39(14), 2611–2622.

13. Younis, H. F., Kaazempur-Mofrad, M. R., Chan, R. C., Isasi, A. G., Hinton, D. P., Chau, A. H., Kim, L. A., Kamm, R. D., Hemodynamics and wall mechanics in human carotid bifurcation and its consequences for atherogenesis: investigation of inter-individual variation. *Biomech Model Mechanobiol* **2004,** 3(1), 17–32.

14. Aletras, A. H., Ding, S., Balaban, R. S., Wen, H. Displacement Encoding in Cardiac Functional MRI, In *Proceedings of the 6th Annual Meetings of ISMRM*, Sydney, Australia, **1998**; p 281.

15. Aletras, A. H., Balaban, R. S., Wen, H., High-resolution strain analysis of the human heart with fast-DENSE. *J Magn Reson* **1999,** 140(1), 41–57.

16. Aletras, A. H., Ding, S., Balaban, R. S., Wen, H., DENSE: displacement encoding with stimulated echoes in cardiac functional MRI. *J Magn Reson* **1999,** 137(1), 247–252.

17. Soellinger, M., Rutz, A. K., Kozerke, S., Boesiger, P. Time-resolved, three-dimensional brain motion measurements using 3D-DENSE, In *Proceedings of the 15th Annual Meeting of ISMRM*, Berlin, Germany, **2007**; p 3005.

18. Wen, H., Vignaud, A., Rodriquez, I., Regional strain mapping of the carotid artery wall in Humans using DENSE. *Magn Reson Mater Phy* **2005,** 18(S1), S60–S61.

19. Aletras, A. H., Wen, H., Mixed echo train acquisition displacement encoding with stimulated echoes: an optimized DENSE method for in vivo functional imaging of the human heart. *Magn Reson Med* **2001,** 46(3), 523–534.

20. Bennett, E., Pai, V. M., Wen, H., Ultrafast Dense Technique for Mapping the Volumetric 3D Wall Motion of the Left Ventricle. In *Proceedings of the 10th Annual Meeting of ISMRM*, Honolulu, Hawaii, **2002**; p 775.

21. Kim, D., Kellman, P., Improved cine displacement-encoded MRI using balanced steady-state free precession and time-adaptive sensitivity encoding parallel imaging at 3 T. *NMR Biomed* **2007**, 20(6):591–601.

22. Wen, H., Rodriquez, I., Bennett, E., Vignaud, A., Optimization of DENSE Sequence for Imaging Regional Strain Distribution in the Carotid Artery Wall and Preliminary Tests in Humans. *J Cardiovasc Magn Reson* **2006,** 8(1), 153–154.

23. Callot, V., Bennett, E., Decking, U. K., Balaban, R. S., Wen, H., In vivo study of microcirculation in canine myocardium using the IVIM method. *Magn Reson Med* **2003,** 50(3), 531–540.

24. Epstein, F. H., Gilson, W. D., Displacement-encoded cardiac MRI using cosine and sine modulation to eliminate (CANSEL) artifact-generating echoes. *Magn Reson Med* **2004,** 52(4), 774–781.

25. Bennett, E., Spottiswoode, B., Lorenz, C. H., Wen, H., Optimal Combination of Phase Cycling and Gradient Spoiling in DENSE Displacement Mapping. In *Proceedings of the 14th Annual Meeting of ISMRM*, Seattle, Washington, **2006,** p. 1649.

26. Fung, Y. C., *Biomechanics : mechanical properties of living tissues*. 2nd ed.; Springer-Verlag: New York, 1993; p xviii, 568 pgs.

27. Crowe, L. A., Ariff, B., Keegan, J., Mohiaddin, R. H., Yang, G. Z., Hughes, A. D., Mc, G. T. S. A., Firmin, D. N., Comparison between three-dimensional volume-selective turbo spin-echo imaging and two-dimensional ultrasound for assessing carotid artery structure and function. *J Magn Reson Imaging* **2005,** 21(3), 282–289.

28. Leeson, C. P., Robinson, M., Francis, J. M., Robson, M. D., Channon, K. M., Neubauer, S., Wiesmann, F., Cardiovascular magnetic resonance imaging for non-invasive assessment of vascular function: validation against ultrasound. *J Cardiovasc Magn Reson* **2006,** 8(2), 381–387.

29. Oyre, S., Ringgaard, S., Kozerke, S., Paaske, W. P., Erlandsen, M., Boesiger, P., Pedersen, E. M., Accurate noninvasive quantitation of blood flow, cross-sectional lumen vessel area and wall shear stress by three-dimensional paraboloid modeling of magnetic resonance imaging velocity data. *J Am Coll Cardiol* **1998,** 32(1), 128–134.

30. Riley, W. A., Evans, G. W., Sharrett, A. R., Burke, G. L., Barnes, R. W., Variation of common carotid artery elasticity with intimal-medial thickness: the ARIC Study. Atherosclerosis Risk in Communities. *Ultrasound Med Biol* **1997,** 23(2), 157–164.

31. Dijk, J. M., Algra, A., van der Graaf, Y., Grobbee, D. E., Bots, M. L., Carotid stiffness and the risk of new vascular events in patients with manifest cardiovascular disease. The SMART study. *Eur Heart J* **2005,** 26(12), 1213–1220.

32. Safar, M. E., Blacher, J., Mourad, J. J., London, G. M., Stiffness of carotid artery wall material and blood pressure in humans: application to antihypertensive therapy and stroke prevention. *Stroke* **2000,** 31(3), 782–790.

33. Roman, M. J., Devereux, R. B., Schwartz, J. E., Lockshin, M. D., Paget, S. A., Davis, A., Crow, M. K., Sammaritano, L., Levine, D. M., Shankar, B. A., et al., Arterial stiffness in chronic inflammatory diseases. *Hypertension* **2005,** 46(1), 194–199.

34. Scuteri, A., Brancati, A. M., Gianni, W., Assisi, A., Volpe, M., Arterial stiffness is an independent risk factor for cognitive impairment in the elderly: a pilot study. *J Hypertens* **2005,** 23(6), 1211–1216.

35. Ribbers, H., Lopata, R. G., Holewijn, S., Pasterkamp, G., Blankensteijn, J. D., de Korte, C. L., Noninvasive two-dimensional strain imaging of arteries: validation in phantoms and preliminary experience in carotid arteries in vivo. *Ultrasound Med Biol* **2007,** 33(4), 530–540.

Chapter 3: Single-Shot DENSE

Abstract

Displacement-encoding with stimulated-echoes (DENSE) MRI provides quantitative strain measurements of the biomechanical function of vessel wall motion. I initially applied this method to the carotid arteries using a true-FISP segmented k-space readout and phase cycling signal averaging to improve SNR and remove unwanted FID and stimulated-antiecho signals. While it has been proven effective for validation of strain in the common carotid arteries, in-plane flow artifacts are pronounced at and above the bifurcation of the carotid arteries where blood flow is faster and more turbulent. The goal of the current study is to compare the previously validated segmented sequence with the single-shot implementation in both *in vitro* and *in vivo* scans. Results show that the single-shot sequence with rigid body image registration is less susceptible to in-plane flow artifacts, particularly above the bifurcation, and motion artifacts due to swallowing and neck motion, which increases the reproducibility and accuracy of strain measurements in the carotid arteries. This allows for optimal *in vivo* characterization of atherosclerotic plaque in future studies.

Introduction

Atherosclerosis, the buildup of plaque in the blood vessels, has been shown to present at distinct regions of arteries, primarily at areas of bifurcation where the main artery splits into one or more smaller arteries [1, 2]. The carotid arteries are one such region where atherosclerotic plaque tends to accumulate that is of great concern because these culprit carotid plaques can lead to stroke [3-6]. Furthermore, atherosclerosis in the carotid arteries has also been linked to cardiovascular disease [7, 8] and in particular myocardial infarction [9-11]. Central to both stroke and heart attack is the fact that currently there is no method that can identify those plaques most likely to rupture causing cerebral or myocardial infarction, the so-called vulnerable plaques [12]. It is recognized that the biomechanical properties of plaque should be predictive of vulnerability [13, 14]. While a number of methods based on biomechanics such as measuring aterial distensiblity, compliance, and stiffness index have been proposed [15, 16], all of them assume that the arteries are axisymmetrical which can not account for the more complex geometry induced by the presence of plaques. A method that can pinpoint specific biomechanical properties in the plaque is required. We have shown and validated in a previous study that a noninvasive method using displacement-encoding with dtimulated-echoes magnetic resonance imaging (DENSE-MRI) can define strain in the carotid arteries. This strain may provide the much-needed marker for plaque vulnerability.

The DENSE-MRI method takes advantage of the stimulated echo which maintains phase information in the longitudinal direction that does not decay as quickly as in the transverse plane. The encoding and decoding gradient pulses are separated by the mixing time TM, so that spin displacement during this time causes a phase shift in the

acquired image which is proportional to the net displacement in the direction of the gradient. This method has been applied to the carotid arteries using a true fast imaging with steady-state (true-FISP) segmented k-space readout and phase cycling signal averaging to improve signal-to-noise ratio (SNR) and remove unwanted free induction decay (FID) and stimulated-anti-echo signals [17, 18].

While DENSE-MRI has been proven effective for validation of strain in the common carotid arteries, through-plane flow artifacts are sometimes pronounced at and above the bifurcation of the carotid arteries where blood flow is more turbulent. Slow through-plane flow signal may not be completely crushed at the end of the acquisition which would result in flow artifacts. Also, refocused magnetization in flowing blood from beat to beat due to its relatively long T1 can cause ringing effects in the images in the segmented acquisition. Furthermore, off-resonance effects from the difference in fat and tissue, particularly pronounced due to the fat alongside the neck can also cause artifacts. Additional artifacts can be seen with segmented k-space acquisition and signal averaging from mis-registration of segmented scans caused by movement such as swallowing. An *in vivo* image shown in figure 3.1 reflects the results of these artifacts. These problems are critical because atherosclerosis tends to build at the bifurcation, and therefore accurate strain mapping must be achieved for this method to be of clinical value. The solution to these problems is to implement a single-shot imaging method and rigid body image registration in postprocessing which has been used in

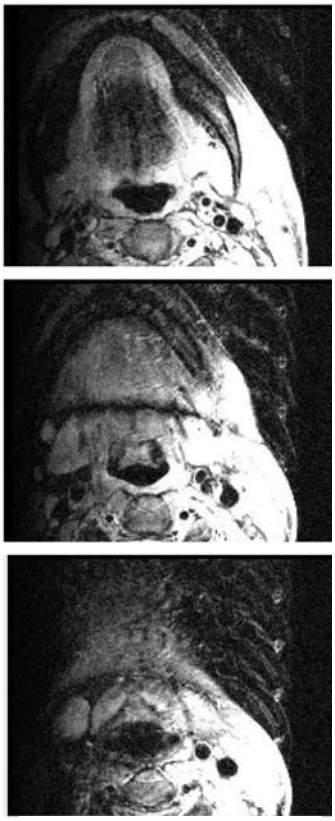

Figure 3.1 *In vivo* DENSE phase maps demonstrating in-plane flow artifacts and ringing-artifacts.

cardiac DENSE applications to allow for free-breathing acquisitions [19, 20]. Single-shot imaging is not influenced by differences in flow from segment to segment as a complete scan is achieved in a single acquisition. Motion artifacts can be eliminated by rigid-body coregistration. The purpose of this study is to implement a single-shot based DENSE pulse sequence and quantitatively compare segmented and single-shot DENSE strain measurements in phantoms and human subjects.

Methods

Phantom System

To model the carotid arteries, previous work has demonstrated that polyvinyl alcohol cryogel (PVA-C) is an ideal material for building phantoms not only due to similar biomechanical properties, such as elasticity, but also anthropomorphic MRI properties, such as T1, T2, and chemical shift [21]. Annular polycarbonate molds were created with a polycarbonate tube with an inner diameter of 0.25 inch and polycarbonate rod with an outer diameter of 0.125 inch yielding 0.125 inch wall thickness. A 10% solution of PVA-C was then liquefied, heated, and poured into the mold as described in previous papers [22]. The molds were frozen at -20° C for 16 hours and thawed at room temperature for 8 hours. The PVA-C elasticity was dependent on the number of freeze-thaw cycles due to increased binding of the gel matrix [21] therefore the phantoms underwent five freeze-thaw cycles. The phantoms were then removed from the mold and stored in anionic water. At the time of imaging, the phantoms were attached to a holder that was filled with water so that the phantom was immersed. Tubing was used to attach the phantom to a pressure gauge and to a pulsatile blood pump (Model #1423, Harvard Apparatus, Boston, MA) from one end to the other, forming a circular loop (see Figure

3.2). The tubing was then filled with water to a pressure of 47 mmHg. The pump was then turned on and gated to a ±5 mV output that mimics EKG gating in human data acquisition. The phantom was imaged on a 3T clinical MR scanner (Trio, Siemens, Germany) using a 3.5 m receive-only surface coil (Nova Medical, Wilmington, MA) that lay under the phantom holder. CINE MRI and segmented and single-shot DENSE MRI are described below.

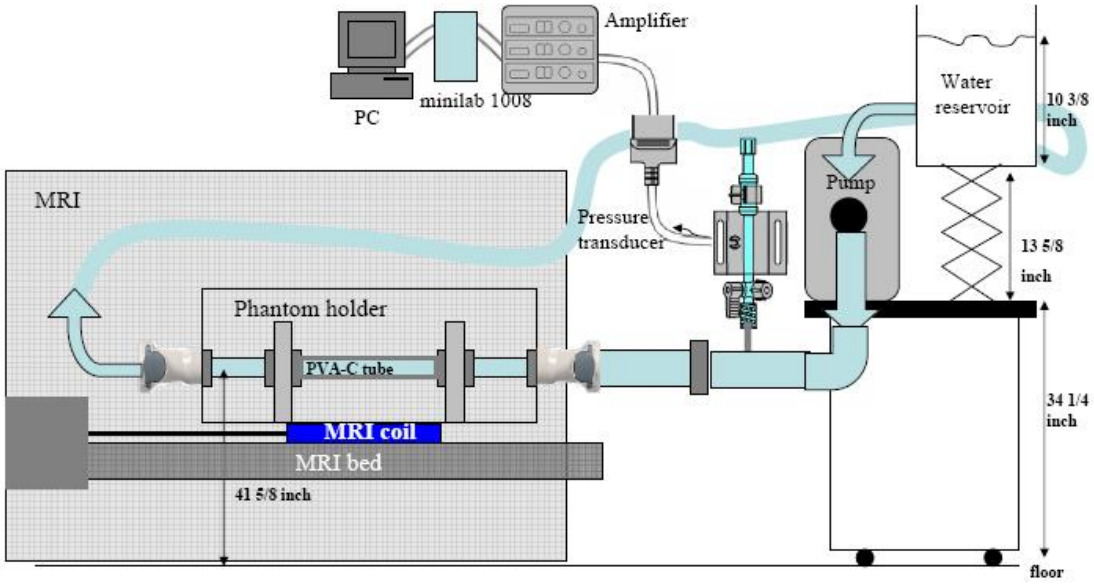

Figure 3.2 *In vitro* setup. Representative images of the phantom experiment setup. Not drawn to scale.

Imaging Protocol

The imaging protocol for both *in vitro* and *in vivo* studies utilized the following sequences: First, a rapid three plane true-FISP localizer was used to localize the coil and ensure proper placement of the coil relative to the phantom or carotid arteries. Second, a three-dimensional (3D) multislab time-of-flight (TOF) MRI was acquired to localize the left and right carotid arteries and identify the bifurcation using maximum intensity projections (MIP) in sagittal and coronal views. Third, CINE MRI was acquired using

2D FLASH with TR = 20/40 ms and TE = 4.4/3.4 ms for 1.5T and 3T field strength, respectively. Three 4 mm thick slices were prescribed on the MIP reconstructed images that were perpendicular to the common carotid artery, centered at the bifurcation, and spaced 9 mm apart as shown in Figure 3.3. Therefore the first slice was placed at 1 cm below the bifurcation of the carotid arteries in the common carotid, the second slice at the bifurcation, and the third slice at 1 cm above the bifurcation to include the internal and external arteries. In the *in vitro* studies, three slices were placed at the center of the phantom. These same slice locations were used for the segmented and single-shot DENSE acquisitions. A total of 36 phases were acquired with 0.6 * 0.6 * 4 mm^3 resolution.

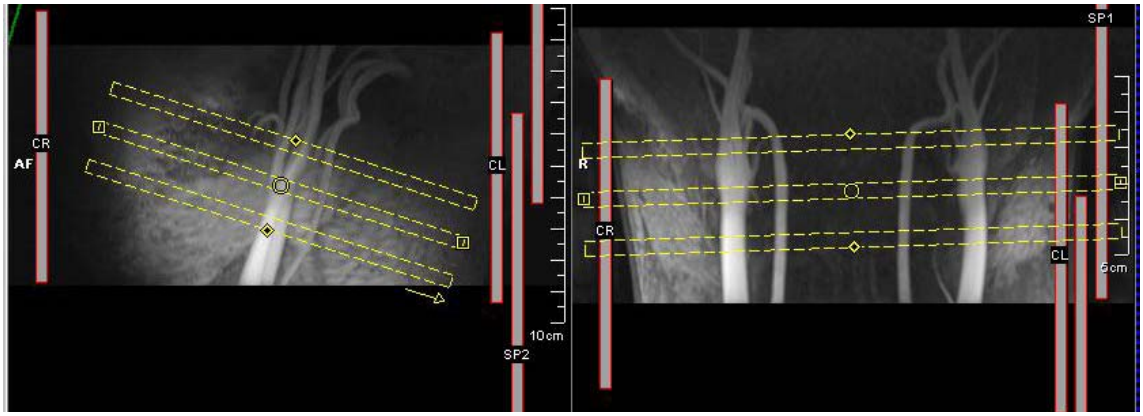

Figure 3.3 Slice locations for CINE and DENSE acquisitions.

The segmented DENSE scans were triggered by the R-wave of the ECG which initiates the first 90° excitation followed by an encoding gradient lobe with an area of 0.60 π/mm inplane that disperses the phase along a defined direction. A second 90° RF pulse is then applied to transfer the magnetization to the longitudinal axis. The decoding gradient pulse is played 100 ms later thus providing the mixing time for the stimulated echo such that the phase dispersion is rewound to the transverse plane. Imaging was then

performed with slice selection using a trueFISP readout of 24 k-space lines per heartbeat acquired over 10 segments, thereby providing 240 phase encoding lines. A matrix size of 256 * 240 was therefore acquired in a 204.8 * 192 mm field of view to provide a resolution of 0.80 * 0.80 * 4mm at 1.5T. At 3.0T images were acquired at 0.60 * 0.60 * 4mm resolution but in postprocessing, the resolution was interpolated to match the 0.80 * 0.80 mm resolution used at 1.5T and in the single-shot DENSE sequence described below. A bandwidth of 585Hz per pixel was used with, TR/TE = 4.8/2.4 ms, and flip angle of 15 degrees. Signal averaging, or phase cycling, of 5 was used. Displacement encoding was acquired in three oblique directions ([0, 1, 1], [0, -1, 1], [1, 0, 1]) to produced a pixel-by-pixel 2D displacement map.

The single-shot DENSE sequence also employed a true-FISP readout however using 64 k-space lines per heartbeat at TR = 3.06 ms with a 30 degree flip angle. A restricted FOV excitation in the phase-encoding direction by the DENSE-encoding RF pulses created an equivalent FOV of 102.4 * 205 mm and 128x256 matrix thereby providing an in-plane resolution of 0.8 * 0.8 * 4.0 mm. A trigger interval of 2 heartbeats was used. As with the segmented DENSE, three different oblique directions were acquired to produce the 2D displacement map. The three separate encoding directions were acquired in 3 separate heartbeats. 48 repetitions were acquired for each direction for a scan time of 4.8 minutes for each slice and a total of 144 shots. The segmented DENSE scan required a comparable scan time of 5 minutes per slice and based on 10 segments, 3 directions, and 5 phase cycles, an equivalent total of 150 shots.

For the *in vivo* study four healthy volunteers (3M, 1F, ages 33-40) were scanned at 1.5T (Siemens Avanto) and an additional four healthy volunteers (2M, 2F, ages 21-50) were scanned at 3.0T. Subjects were screened for MR contraindications and history of

cardiovascular and neurological disease and informed consent was obtained under IRB-approved protocols. Field-strength specific bilateral dual phased array carotid coils (Machnet, Netherlands) were used for imaging at both 1.5T and 3T. Semiautomated shimming was acquired before segmented and single-shot slice acquisitions over a volume larger than FOV. In order to ensure that there was no effect from shimming alone, segmented and single-shot acquisitions were alternated in order between subjects.

Image Processing

The DENSE raw data was downloaded from the MR scanners and processed using custom software (DENSEview, NIH, Bethesda, MD) to extract strain maps and quantitative strain measurements for each slice. Data processing methods are described in detail in the previous validation paper [18] and in [23], however an additional step for handling of the single-shot data is described: First, multichannel complex images are combined into three sets encoded in the X, Y, and Z direction. For single-shot data, image coregistration of each shot was done by calculating the Pearson's correlation coefficient of all pairs of frames to identify the frame with the highest total correlation which was used as the reference frame. Each individual frame was then registered by X and Y translations until the maximum Pearson's correlation were reached [24]. The frames are ordered by correlation and displayed frame by frame in a movie. The user can then select a percentage of frames to be included and averaged. In most cases, 90% of the frames were utilized in this study except where specified. The advantage of this additional coregistration step is that in those data acquisitions where there is motion, those frames that exhibit residual motion after registration will have a low Pearson's correlation. If there is a great deal of residual motion, for example affecting nearly half

of the frames, the user can then select to use only 50% of the frames thereby eliminating registration artifacts in the single-shot images. This step is not possible in the segmented DENSE scans. The following postprocessing steps remain the same for both single-shot and segmented DENSE scans: Second, an ROI is selected by the user to define the common carotid, bifurcation, or internal carotid artery depending on the slice being analyzed. Contours defining the carotid lumen wall are drawn by the user. Adaptive phase unwrapping [23] was then performed on the phase maps and converted to X, Y, and Z displacement as a vector. An adaptive spatial filter is applied and a displacement map is created. Circumferential strain (E_{cc}) maps were calculated as a projection of the Lagrangian strain tensor based on a tissue deformation matrix from the in-plane displacement of each quadrilateral element.

Mean E_{cc} was calculated by taking the average of the pixel values over a contour drawn around the lumen wall at three slices 1 cm apart at the center of the phantom for the *in vitro* study and at the common carotid artery and internal common carotid artery slices for the *in vivo* study. Variance of strain around the lumen was obtained as a whole as well as in four different segments of the image. CINE E_{cc} was obtained by measuring and multiplying the horizontal and vertical lumen diameter at two time points that match the beginning (systolic) and acquisition (diastolic) time points of the segmented and single-shot DENSE scans divided by the lumen diameter at the end (diastolic) time point. At 1.5T the CINE MRI lumen diameter measurements were taken at time-to-trigger TT = 0 ms and TT = 190 ms for comparison to segmented DENSE and TT = 290 ms for single-shot DENSE and at 3T the segmented DENSE diastolic time point was at TT = 260ms and single-shot TT = 320 ms. The difference in the diastolic time points is due to the longer imaging window required for single-shot DENSE which acquires 64 k-space lines

as opposed to 24 k-space lines for segmented DENSE as described above. Finally, signal-to-noise ratio was calculated based on the lumen wall for signal and an additional ROI was drawn by the user in the center of lumen to determine the noise level, giving signal-to-noise ratio and its variance around the lumen.

Results

Phantom Studies

Phantom studies using true-FISP readout showed a nearly two times SNR increase over using a FLASH readout. Initial phantom and *in vivo* studies showed that a flip angle of 30° is optimal at both 1.5T and 3.0T. In phantoms, inplane flow artifacts were evident in segmented DENSE images but not single-shot DENSE images as shown in figure 3.4a. The phase maps show that single-shot DENSE does not suffer from these artifacts. The effect of the artifacts can also be visualized in the strain map which shows that voxels along the artifact show inaccurate high strain values whereas the single-shot DENSE shows the expected uniform strain values throughout the phantom wall. This improvement can be quantified by the lower variability of repeated strain measurements and lower standard deviation of intravoxel strain measurements (figure 3.4b) which reflects a greater reproducibility and accuracy with the single-shot DENSE sequence.

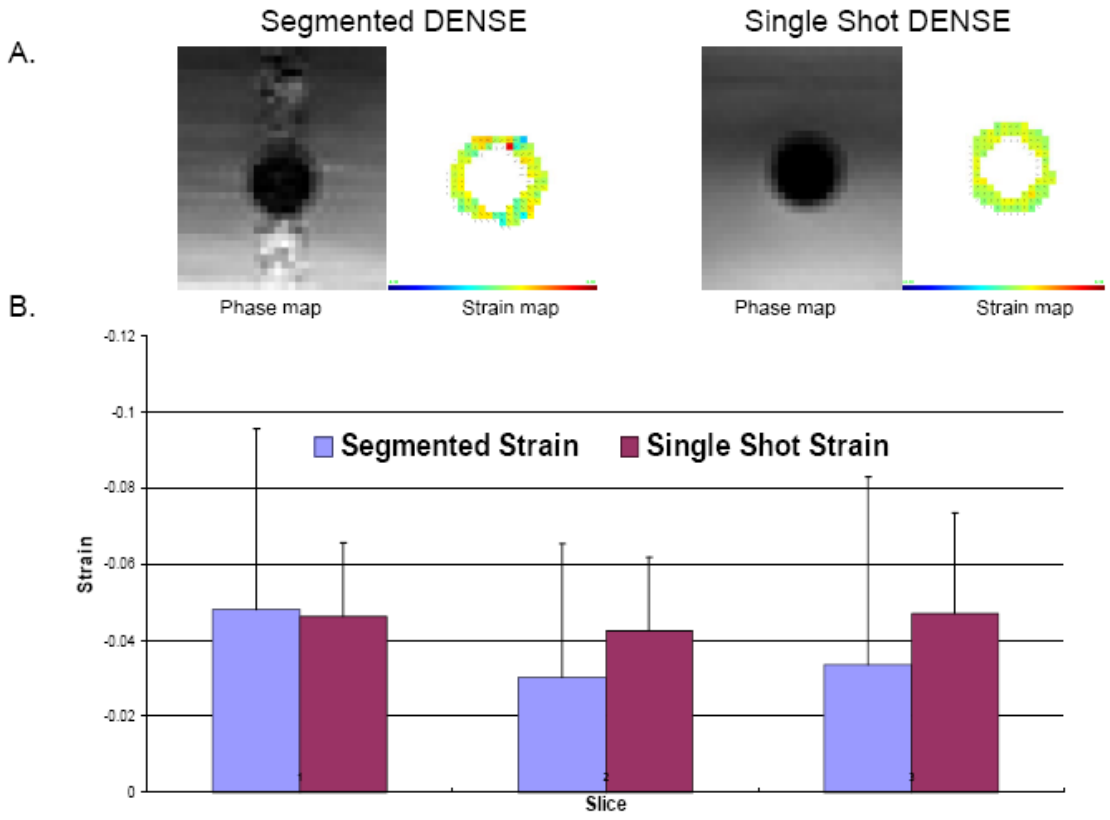

Figure 3.4. In vitro comparison of segmented and single-shot DENSE. A) Phase maps and strain maps of phantoms with segmented DENSE (left) and single-shot DENSE (right). B) Average strain and standard deviation measurements across the phantom wall in segmented and single-shot DENSE.

Studies *In Vivo*

These results are also reflected in the *in vivo* studies as shown in figure 3.5 which shows irregular displacement vectors in segmented DENSE at the bifurcation that are likely the result of image artifacts whereas the single-shot DENSE displacement and strain map reflects displacement in the expected directions. However, in order to quantify accuracy of the DENSE scans, E_{cc} values were obtained in both segmented and single-shot DENSE slices at the common carotid arteries and internal carotid artery and compared with E_{cc} measurements obtained from CINE MRI from the same slice locations. The bifurcation was excluded from this analysis due to complex geometry that is not well represented by taking the average of Ecc across the lumen wall.

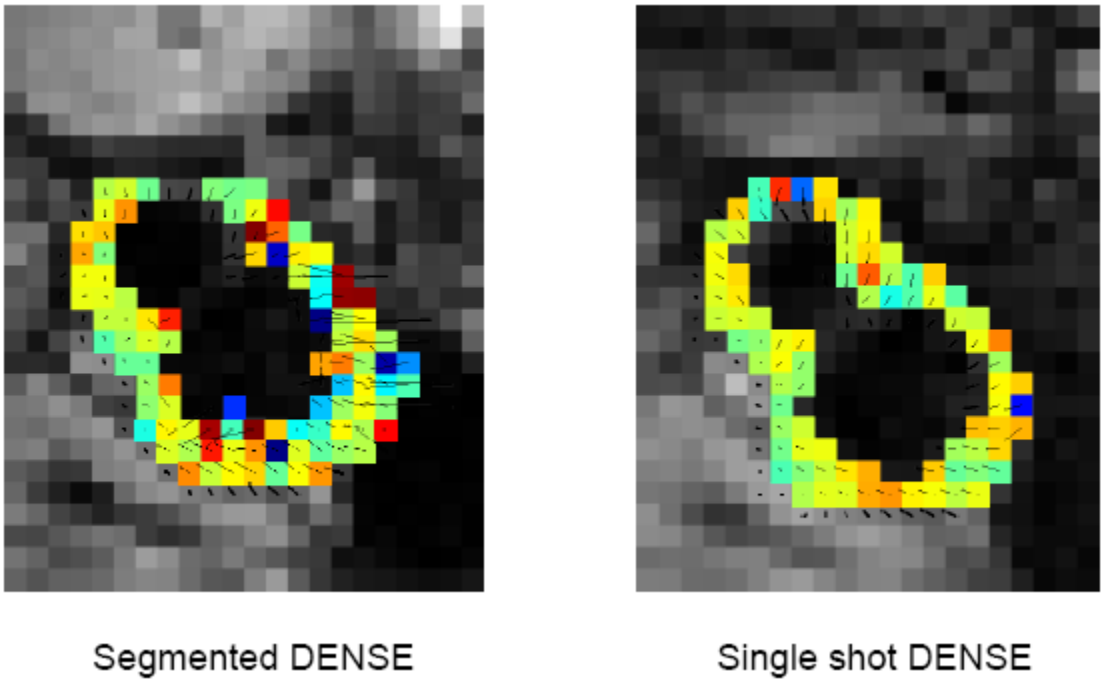

Figure 3.5 *In vivo* comparison of segmented and single-shot DENSE displacement and strain maps.

At 1.5T, the Pearson's correlation (r^2) between the CINE and DENSE E_{cc} was 0.76 and 0.95 for segmented and single-shot DENSE, respectively. The slopes of linear regression were 0.63 ± 0.20 (95% confidence interval, CI) and 0.81 ± 0.11 (95% CI), respectively. The 1.5 T results are shown in the correlation graph in figure 3.6.

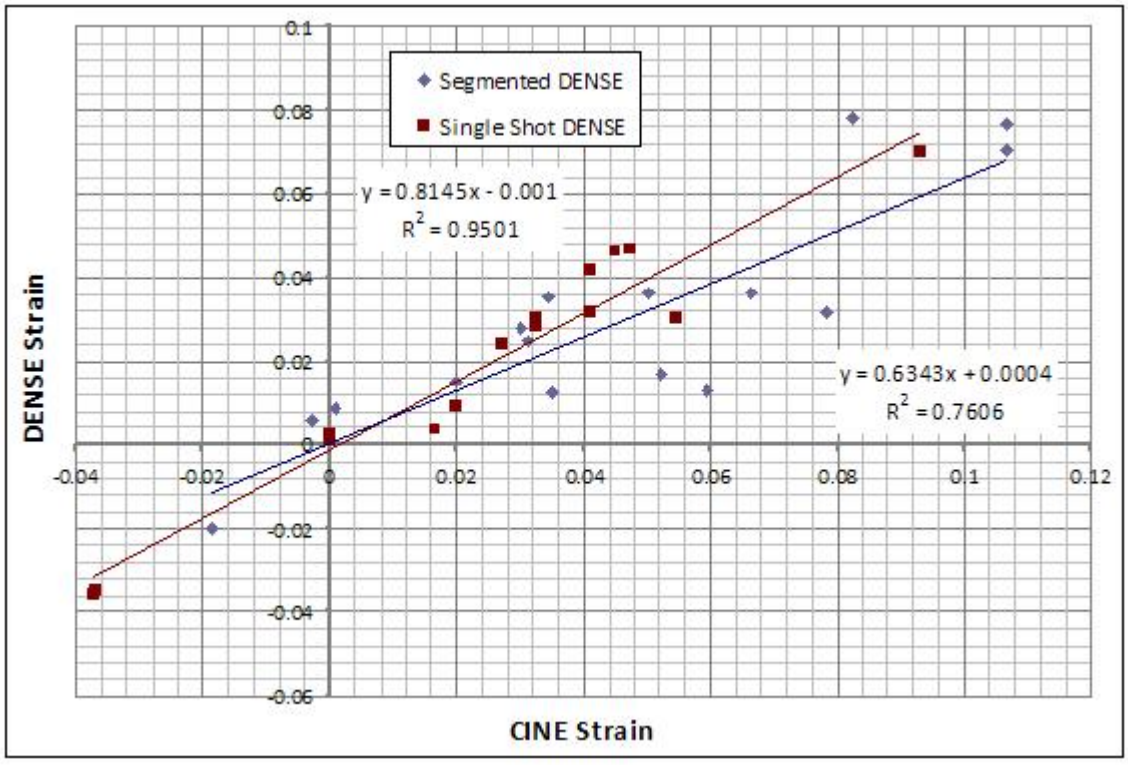

Figure 3.6. CINE and DENSE circumferential strain correlation at 1.5T.

At 3.0T, the segmented DENSE E_{cc} showed a much lower Pearson's correlation of 0.68 with CINE Ecc compared to single-shot DENSE E_{cc} correlation of 0.91 (figure 3.7). The slopes of regression were 1.02 ± 0.40 (95% CI) and 0.88 ± 0.16 (95% CI), for segmented and single-shot DENSE, respectively. The zero intercepts were -0.018± 0.016 (95% CI) and 9E-5 ± 0.004 (95% CI), respectively. In the segmented scan the negative intersect was caused by several data points with negative DENSE Ecc but positive CINE Ecc.

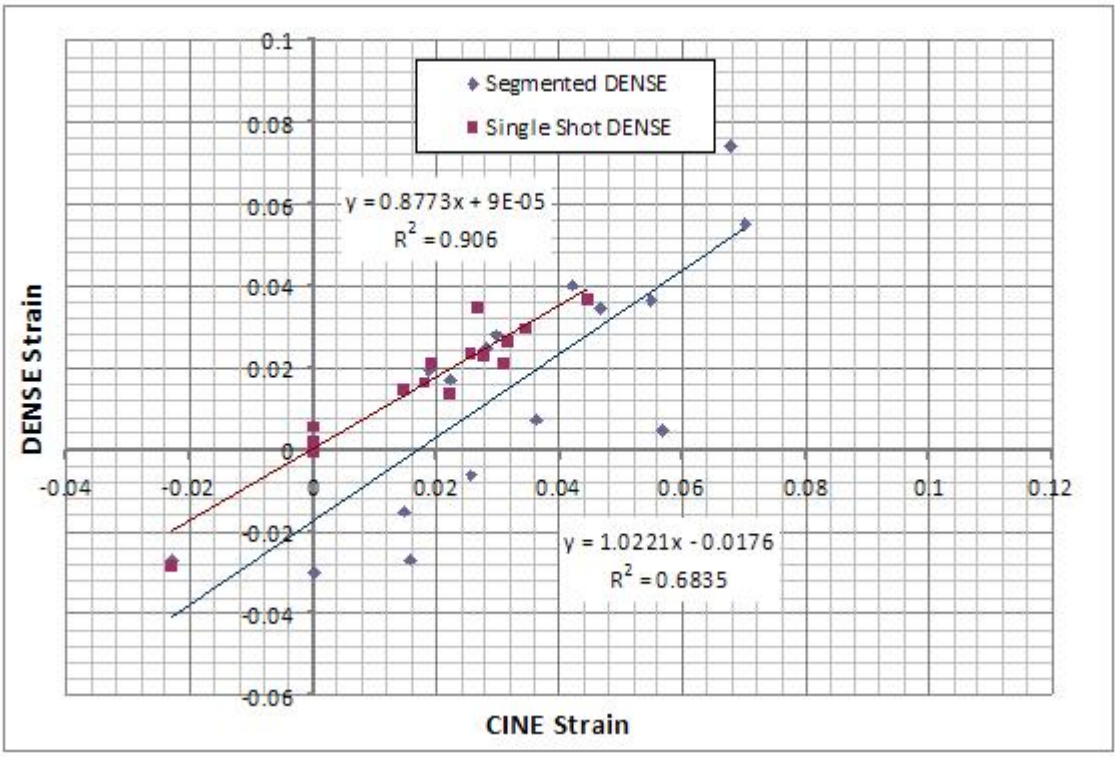

Figure 3.7. CINE and DENSE circumferential strain correlation at 3T.

A closer examination of these points reveal that they are from the common carotid artery of a single subject where segmented DENSE scans suffered from significant artifacts that caused portions of the phase map to be distorted (Figure 3.8). As shown in the phantom experiments, this resulted in inaccurate strain calculations. This example also demonstrates the dramatic improvement of image quality with the single-shot DENSE implementation as evidenced by the well-defined morphology of the single-shot phase maps compared to the segmented data in the same subject. Although the samples are different from 1.5T and 3.0T, the results seem to support that segmented DENSE measurements are not as accurate at 3.0T when compared to 1.5T. This is likely due to the well-described increases in susceptibility and chemical shift dispersion at 3.0T [25].

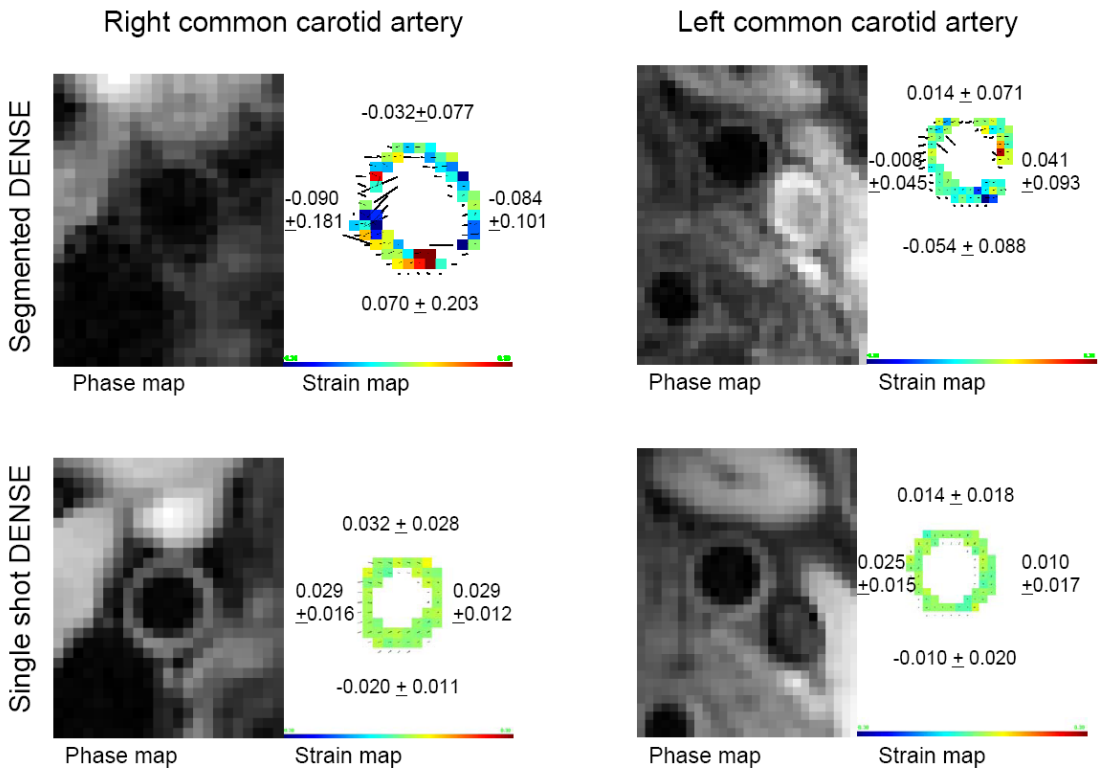

Figure 3.8 Phase map and strain map and values of common carotid arteries in a subject that showed contradictory CINE Ecc and segmented DENSE Ecc strain values. Strain value and standard deviation for each quadrant of the lumen wall are shown.

Another means by which single-shot DENSE improvements can be quantified is by examining the improvement in SNR when compared to segmented DENSE scans. In order for the SNR to comparable in segmented and single-shot DENSE scans, the SNR per shot was calculated and a pair-wise comparison was made for each side, slice, and subject. At 1.5T the mean SNR for segmented scans was 8.7 $\pm$ 7.4 which was significantly lower ($p<0.005$) than SNR for single-shot of 21.3 $\pm$ 18.3 thereby showing a nearly three times increase in DENSE SNR by using the single-shot implementation. As shown in Figure 3.9, in all but one measurement, SNR was increased when using single-shot DENSE for all measurements in all subjects. At 3.0T, the mean SNR for segmented scans was 8.9 $\pm$ 6.3 which was also significantly lower ($p<0.05$) than single-shot scans

with a mean SNR of 14.8 $\pm$ 10.1. In pair-wise comparisons, four locations showed lower SNR with single-shot scans.

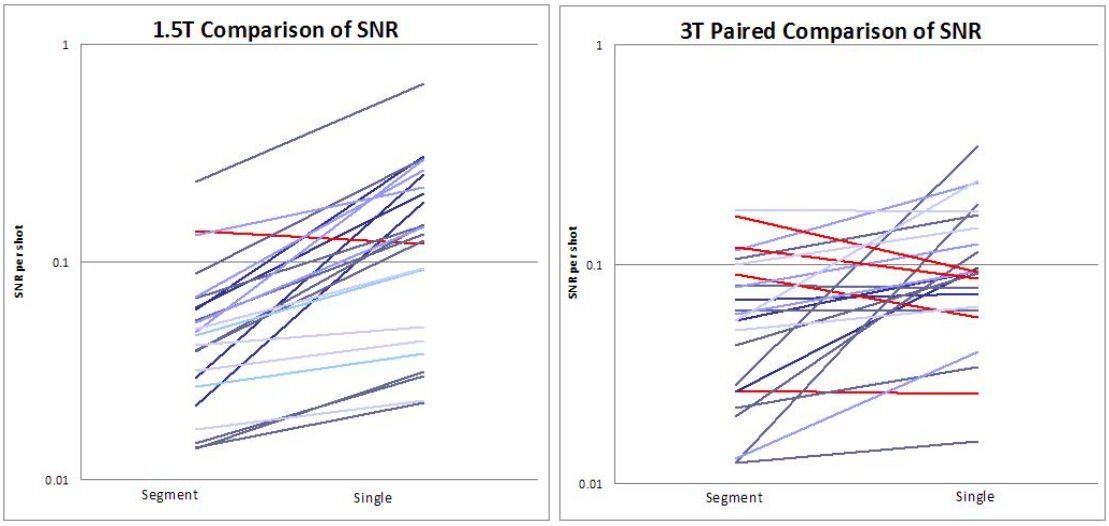

Figure 3.8 Pair-wise SNR comparisons of segmented DENSE and single-shot DENSE at 1.5T and 3T

The five measurements that showed lower SNR with single-shot DENSE were examined in more detail. The data reconstruction showed that using 90% of the images for the rigid body coregistration algorithm still resulted in images with residual motion as shown in Figure 3.10 (top left). To take advantage of the flexibility of the coregistration algorithm, the data was postprocessed using a lower fraction of images with the goal of removing those frames with residual motion. In some cases, as much as 50% of the single-shot frames were removed in order to rid the scan of artifacts. The plot shown in Figure 3.10 demonstrates that by reducing the number of frames used for averaging, one can in fact increase the SNR by removing the contributing noise from residual motion and other artifacts. The increase in SNR is reflected in the DENSE images where in the initial data processing (top left) used 90% of the frames, the re-processed data using 60% of the frames reveal vessel morphology that was not discernable in the initial image.

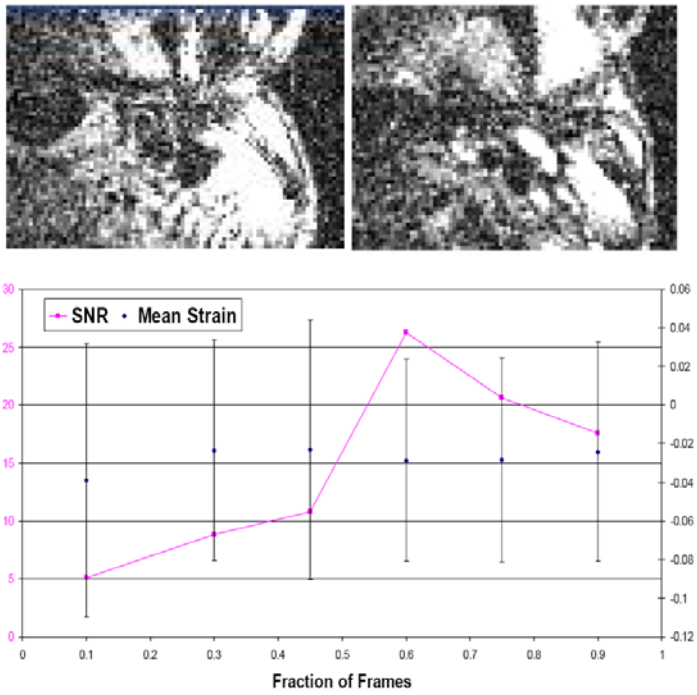

Figure 3.10 Top left: Single-shot DENSE scan with 90% of the frames used for averaging. Top right: Single-shot DENSE scan with 60% of the frames used for averaging. Botttom: SNR and strain measurements using 10%, 30%, 45%, 60%, 75%, and 90% of the single-shot frames in the same subject and slice location.

By reprocessing the five cases using fewer frames, the SNR was improved by 3% at 1.5T and 13.5% at 3.0T. In all five cases, SNR of single-shot DENSE now shows improvement over segmented DENSE SNR as shown in Figure 3.11.

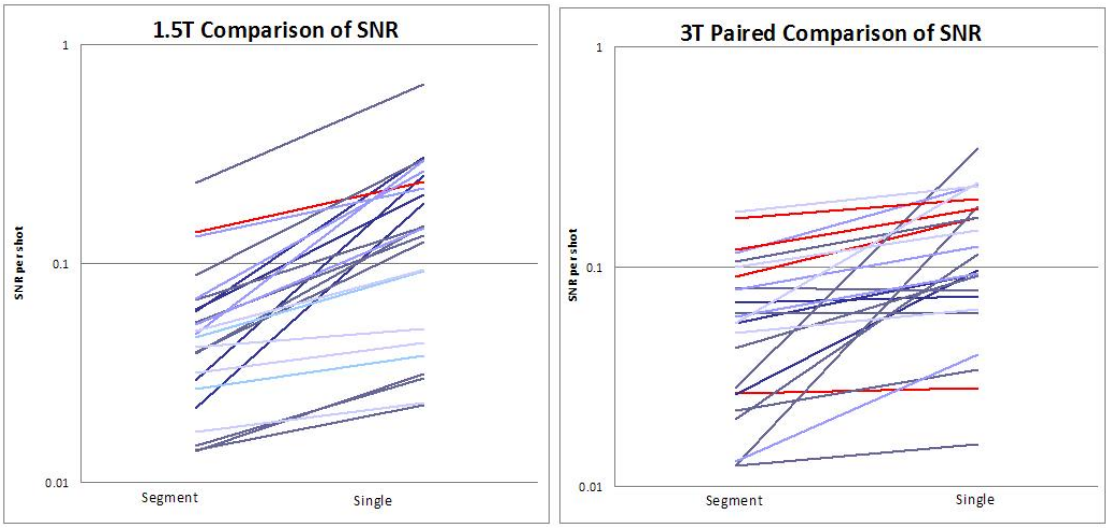

Figure 3.11 Pair-wise SNR comparisons of segmented DENSE and single-shot DENSE at 1.5T and 3.0T after reprocessing using fewer frames in the coregistration algorithm.

Discussion

The single-shot DENSE implementation shows improvement in accuracy and SNR by effectively eliminating artifacts arising from head-neck motion and in-plane flow at and above the bifurcation of the carotid arteries. Although there is an additional step in postprocessing which takes an extra minute or two to accomplish per slice, the improvement in SNR by nearly 300% outweighs the extra time. The additional step of image coregistration provides a more flexible protocol that is tolerant of motion artifacts such as swallowing and patient movement which can not be controlled. By using a single-shot sequence a more robust protocol can be provided for future studies.

One of the drawbacks to the accuracy comparison was the limitation of the CINE E_{cc} measurements. Unfortunately, another method of validating DENSE measurements does not exist as it is the only MR imaging method that has been shown to measure strain in the carotid arteries. Other displacement-encoding method such as tagging or HARP do not have the resolution necessary for carotid imaging [26]. The only known method for measuring circumferential strain *in vivo* is the use of intravascular ultrasound [27] however it is not only invasive but it would be difficult to coregister the strain measurements with MR measurements.

It is tempting to compare SNR measurements at 1.5T and 3.0T. Although the SNR improvement is shown by single-shot DENSE at both field strengths, it is surprising that the SNR at 3T was not significantly greater ($p>0.05$) than the SNR at 1.5T as observed in the previous validation study [18]. It is important to note that subjects scanned at 1.5T were different from those scanned at 3.0T. The 3.0T subjects were less experienced inside an MR scanner. This may have resulted in greater motion and therefore more artifacts that would have decreased SNR. A more likely explanation for

the lower than expected SNR at 3.0T is that the noise measurements were taken from within the lumen which in the case at 3T may not just be noise but contain real blood signal. Since T1 of blood is longer at 3T, there may be secondary coherence pathways that refocus blood signal from previous shots which has been evidenced in other high-field studies [25]. Also, the 3T group was significantly older ($p<0.05$) which may have resulted in group differences in blood flow patterns. In order to draw conclusive results for a 1.5T and 3.0T comparison, the same subjects must be scanned at both field strengths. However, it can be concluded that DENSE at 1.5T is feasible and that the single-shot DENSE implementation is necessary to have high SNR.

This novel implementation of a single-shot DENSE MRI in the carotid arteries provides a more robust method for measuring strain in all parts of the carotid artery. Future studies will quantify regional strain patterns and compare these patterns in healthy volunteers and patients with known carotid atherosclerosis. These data should show whether regional stiffness of the artery wall is correlated with plaque vulnerability. If so, DENSE-MRI could provide an indication for the risk of stroke, allowing for the early diagnosis of the disease before the devastating effects can take their course.

Acknowledgements

This research was funded by the National Institutes of Health Intramural Research Training Award, American Heart Association Pre-doctoral Fellowship, and the Gordon and Betty Moore Discovery Grant.

References

1. DeBakey, M. E., Lawrie, G. M., Glaeser, D. H., Patterns of atherosclerosis and their surgical significance. *Ann Surg* **1985,** 201(2), 115–131.
2. Thubrikar, M. J., Robicsek, F., Pressure-induced arterial wall stress and atherosclerosis. *Ann Thorac Surg* **1995,** 59(6), 1594–1603.
3. Seeger, J. M., Barratt, E., Lawson, G. A., Klingman, N., The relationship between carotid plaque composition, plaque morphology, and neurologic symptoms. *J Surg Res* **1995,** 58(3), 330–336.
4. Dijk, J. M., van der Graaf, Y., Grobbee, D. E., Bots, M. L., Carotid stiffness indicates risk of ischemic stroke and TIA in patients with internal carotid artery stenosis: the SMART study. *Stroke* **2004,** 35(10), 2258–2262.
5. Mead, G. E., O'Neill P, A., Carotid disease in acute stroke: A review. *J Stroke Cerebrovasc Dis* **1999,** 8(4), 197–206.
6. Agabiti-Rosei, E., Muiesan, M. L., Carotid atherosclerosis, arterial stiffness and stroke events. *Adv Cardiol* **2007,** 44, 173–86.
7. Fernandes, V. R., Polak, J. F., Cheng, S., Rosen, B. D., Carvalho, B., Nasir, K., McClelland, R., Hundley, G., Pearson, G., O'Leary, D. H., et al., Arterial stiffness is associated with regional ventricular systolic and diastolic dysfunction: the Multi-Ethnic Study of Atherosclerosis. *Arterioscler Thromb Vasc Biol* **2008,** 28(1), 194–201.
8. Dijk, J. M., Algra, A., van der Graaf, Y., Grobbee, D. E., Bots, M. L., Carotid stiffness and the risk of new vascular events in patients with manifest cardiovascular disease. The SMART study. *Eur Heart J* **2005,** 26(12), 1213–1220.

9. Johnsen, S. H., Mathiesen, E. B., Joakimsen, O., Stensland, E., Wilsgaard, T., Lochen, M. L., Njolstad, I., Arnesen, E., Carotid atherosclerosis is a stronger predictor of myocardial infarction in women than in men: a 6-year follow-up study of 6226 persons: the Tromso Study. *Stroke* **2007,** 38(11), 2873–2880.

10. Young, W., Gofman, J. W., Tandy, R., Malamud, N., Waters, E. S., The quantitation of atherosclerosis. II. Quantitative aspects of the relationship of blood pressure and atherosclerosis. *Am J Cardiol* **1960,** 6, 294–299.

11. Wofford, J. L., Kahl, F. R., Howard, G. R., McKinney, W. M., Toole, J. F., Crouse, J. R., 3rd, Relation of extent of extracranial carotid artery atherosclerosis as measured by B-mode ultrasound to the extent of coronary atherosclerosis. *Arterioscler Thromb* **1991,** 11(6), 1786–1794.

12. Naghavi, M., Libby, P., Falk, E., Casscells, S. W., Litovsky, S., Rumberger, J., Badimon, J. J., Stefanadis, C., Moreno, P., Pasterkamp, G., et al., From vulnerable plaque to vulnerable patient: a call for new definitions and risk assessment strategies: Part I. *Circulation* **2003,** 108(14), 1664–1672.

13. Burleigh, M. C., Briggs, A. D., Lendon, C. L., Davies, M. J., Born, G. V., Richardson, P. D., Collagen types I and III, collagen content, GAGs and mechanical strength of human atherosclerotic plaque caps: span-wise variations. *Atherosclerosis* **1992,** 96(1), 71–81.

14. Reneman, R. S., Meinders, J. M., Hoeks, A. P., Non-invasive ultrasound in arterial wall dynamics in humans: what have we learned and what remains to be solved. *Eur Heart J* **2005,** 26(10), 960–966.

15. Lehmann, E. D., Terminology for the definition of arterial elastic properties. *Pathol Biol (Paris)* **1999,** 47(6), 656–664.

16. O'Rourke, M. F., Staessen, J. A., Vlachopoulos, C., Duprez, D., Plante, G. E., Clinical applications of arterial stiffness; definitions and reference values. *Am J Hypertens* **2002,** 15(5), 426–444.

17. Lin, A. P., Tyszka, J. M., Bennett, E., Fraser, S., Wen, H., Preliminary Validation of Circumferential Strain Measurements using DENSE at 1.5T and 3T. *J Cardiovasc Magn Reson* **2006,** 8(1), 48–49.

18. Lin, A. P., Bennett, E., Wisk, L., Gharib, M., Fraser, S., Wen, H., Circumferential Strain in the Wall of the Common Carotid Artery: Comparing Displacement-Encoded and CINE MRI in Volunteers. *Magn Reson Med* **2008,** 60(1), 8–13.

19. Le, Y., Kellman, P., Bennett, E., Lin, A. P., Chefd'Hotel, C., Lorenz, C. H., Wen, H., Free-Breathing Single-Shot DENSE Myocardial Strain Imaging Using Deformable Registration. *J Cardiovasc Magn Reson* **2008,** 10(Suppl I), A207.

20. Le, Y., Kellman, P., Taylor, J., Bennett, E., Lucas, K., Chefd'Hotel, C., Lorenz, C. H., Croisille, P., Wen, H., Simultaneous Myocardial Perfusion and Strain Imaging with Displacement-encoded MRI. In *Proc Rad Soc of N Am* **2008,** 94, 382.

21. Chu, K. C., Rutt, B. K., Polyvinyl alcohol cryogel: an ideal phantom material for MR studies of arterial flow and elasticity. *Magn Reson Med* **1997,** 37(2), 314–319.

22. Surry, K. J., Austin, H. J., Fenster, A., Peters, T. M., Poly(vinyl alcohol) cryogel phantoms for use in ultrasound and MR imaging. *Phys Med Biol* **2004,** 49(24), 5529–5546.

23. Wen, H., Marsolo, K. A., Bennett, E. E., Kutten, K. S., Lewis, R. P., Lipps, D. B., Epstein, N. D., Plehn, J. F., Croisille, P., Adaptive postprocessing techniques for

myocardial tissue tracking with displacement-encoded MR imaging. *Radiology* **2008,** 246(1), 229–240.

24. Hermosillo, G., Chefd'Hotel, C., Faugeras, O., Variational Methods for Multimodal Image Matching. *Int J of Comp Vision* **2002,** 50(3), 329–343.

25. Soher, B. J., Dale, B. M., Merkle, E. M., A review of MR physics: 3T versus 1.5T. *Magn Reson Imaging Clin N Am* **2007,** 15(3), 277–290.

26. Kuijer, J. P., Hofman, M. B., Zwanenburg, J. J., Marcus, J. T., van Rossum, A. C., Heethaar, R. M., DENSE and HARP: two views on the same technique of phase-based strain imaging. *J Magn Reson Imaging* **2006,** 24(6), 1432–1438.

27. Schaar, J. A., Regar, E., Mastik, F., McFadden, E. P., Saia, F., Disco, C., de Korte, C. L., de Feyter, P. J., van der Steen, A. F., Serruys, P. W., Incidence of high-strain patterns in human coronary arteries: assessment with three-dimensional intravascular palpography and correlation with clinical presentation. *Circulation* **2004,** 109(22), 2716–2719.

Chapter 4: Age-Related Changes in Strain

Abstract

The loss of elasticity and increased stenosis in the carotid arteries is an unavoidable consequence of aging and is often recognized as an early marker of atherosclerosis, the leading cause of heart attacks and strokes. The purpose of this study was to use magnetic resonance imaging (MRI) as a noninvasive method to measure common carotid artery (CCA) intima-media thickness (IMT) and CCA cyclic strain in normal subjects and patients with atherosclerosis.

30 subjects (18M, 12F, ages 18-79), of which 7 showed atherosclerosis, underwent carotid MR imaging. T1w, T2w, proton-density images, and CINE MRI were acquired and used to measure the IMT and cyclic strain. An additional 20 subjects were examined with DENSE-MRI where cyclic strain was measured by averaging strain across the lumen.

As expected, the results show a general increase in IMT and decrease strain; however a thickened arterial wall did not necessarily confer decreased strain. Age-matched comparisons between stroke and control show a significant difference in strain but not IMT. Also of note is a wide range of cyclic strain in younger controls possibly indicating that strain may precede wall thickening.

The results of this study demonstrate that MRI can be used as a noninvasive tool to measure CCA IMT and elasticity. Combined with high resolution morphological MRI techniques, these measurements can provide a simple method of measuring arterial disease that may add significant value to vulnerable plaque diagnosis.

Introduction

Atherosclerotic cardiovascular disease is the leading cause of death in the United States with over 19 million deaths worldwide where a large portion of these victims are asymptomatic [1]. Therefore there is a considerable demand for the early diagnosis of atherosclerosis, in particular those that are focused on examining atherosclerosis in the carotid wall which is the leading cause of stroke [2]. Atherosclerosis is defined by the hardening or stiffening of the arterial walls therefore a number of diagnostics techniques focus on 1) the morphological changes that occur in the carotid wall such as intima-media wall thickness (IMT) and plaque imaging and 2) the biomechanical changes that arise from stiffening arteries such as distention, cyclic strain, and stiffness.

IMT is the currently accepted surrogate marker for atherosclerosis in the carotid arteries [3]. Numerous large clinical trials including the Rotterdam Study [4, 5] and Atherosclerosis Risk in Communities (ARIC) Study [6, 7] have utilized this technique to determine the relationship of common carotid artery IMT (CCA IMT) with atherosclerosis and more importantly with risk of disease. Their results show that a small increase in CCA IMT of 0.2mm was associated with an increase in relative risk for stroke and heart attack of 28% and 33%, respectively as determined in the ARIC study. IMT is generally measured using B-mode ultrasound (US) by obtaining a side view of the carotid artery and measuring the distance between the leading edges of the lumen-intima and media-adventitia ultrasound interface. While this has been shown to be a reliable and robust measurement, US suffers from variability in operator error (such as tranducer angle) and image artifacts can occur in plaques with calcification [8]. MRI technology has advanced to the point where high resolution images of the IMT can be reliably

obtained [9, 10]. The advantage of using MRI is that other morphological and functional measures of atherosclerosis can be imaged noninvasively as well.

Carotid plaque imaging has recently become available with the advances in imaging hardware and software that enables the characterization of plaque including lipid pool, calcification, hemorrhage, and fibrous tissue [11-13]. Signal intensity in MRI is based on biochemistry of the tissues of interest. Characterization of plaque relies on the premise that different components of plaque will have different signal intensities depending on the method of excitation, otherwise known as the pulse sequence, that focus on different spin relaxation properties. For example, the lipid in plaque has a well known short T_2 (T_2 is the transverse relaxation time of excited spins), therefore T_2-weighted image sequences are more sensitive to lipid than say a T_1-weighted image sequence. Calcification on the other hand has very little proton signal and so it appears dark on all MRI images [12]. By utilizing multiple imaging sequences of variable contrast weighting, plaque can be characterized noninvasively using MRI.

Stiffness of the carotid arteries is implicit in the definition of atherosclerosis and has therefore become a major focus for imaging techniques to measure this biomechanical property [14]. Carotid artery wall stiffness has been implicated in a broad range of cardiovascular and neurological diseases including stroke [15], hypertension [16, 17], heart failure [18], myocardial infarction [19], inflammatory disease [20], cognitive impairment [21], and chronic fatigue syndrome [22]. Furthermore, increased arterial stiffness is directly correlated to increased cardiovascular morbidity and mortality [23]. There are several ways that stiffness can be measured using a number of different techniques. Pulse wave velocity, the measure of time taken by a pressure wave to travel between the carotid artery and femoral artery was primarily used to measure arterial

stiffness, however it suffers from inaccuracies in measurement [24, 25]. Ultrasound is once again used to assess wall function by measuring changes in the lumen diameter. MRI can also be used to measure stiffness by using CINE MRI which acquires rapid images of the carotid artery using the axial plane so that area or diameter of the lumen can be readily measured [11]. The problem with the ultrasound and CINE MRI method of measuring stiffness by change in lumen dimensions is that it assumes that the lumen is expanding and contracting isosymmetrically in order for the calculations to be simple. This is an assumption that has been shown not to be true using displacement encoding with stimulated echo magnetic resonance imaging (DENSE-MRI) which can define localized strain noninvasively [26-28]. DENSE-MRI has been used to measure circumferential strain and therefore can be used to define stiffness.

The terminology used for defining stiffness using these measurements is confusing as different terms are used interchangeably throughout the literature. For the sake of clarity, the following definitions of stiffness are used in this study:

1. Cyclic strain: the change in lumen diameter or area from systole (D_s) to diastole (D_d) as a ratio to the diastolic diameter or area. Referred to in the literature as carotid compliance, distention, and circumferential strain.

$$\varepsilon_{CS} = \frac{D_s - D_d}{D_d} \tag{4.1}$$

2. Circumferential strain: the average of all pixels across the lumen contour (e_c) where each pixel is the tissue deformation matrix for the in-plane displacement as measured by DENSE-MRI. This definition is used in previous publications [28-30] and intended to clarify the difference between cyclic strain and strain measured by DENSE.

$$\varepsilon_{CC} =< e_c^T \frac{(E^T E - 1)}{2} e_c > \quad = 1 - \frac{1}{1 + \varepsilon_{CS}} \tag{4.2}$$

3. Stiffness Index: Ratio of the natural log of the difference in systolic (P_s) and diastolic blood pressures (P_d) relative to the change in diameter or area. This is one measure of stiffness that is universally defined.

$$\beta = \frac{\ln(P_s / P_d)}{(D_s - D_d)/D_d} \tag{4.3}$$

Atherosclerosis is an ongoing process which starts in the first decade of life [31]. As a result, carotid arterial stiffness and thickness has been shown to increase with age, which is supported by ultrasound and pulse-wave velocity studies [23, 32, 33] but has not been explored by MRI measures of stiffness. It is the goal of this study to measure IMT, cyclic strain, circumferential strain, and stiffness index using MRI to determine age-related changes. In addition, a small subgroup of patients with known atherosclerosis will be examined with these methods. The hypothesis is that the measures of stiffness will increase with age and that patients with known atherosclerosis will show significantly different measures of stiffness as measured by MRI. The results of this will demonstrate the feasibility of morphological and mechanical characterization of the carotid arteries using different MRI techniques such that a complete imaging protocol can be developed that would provide all relevant measures of atherosclerosis.

Methods

A total of 50 subjects was examined (ages 18-79, 27 males, 23 females) with carotid imaging. The first group of subjects (n=30, ages 18-79, 18 males, 12 females)

was examined at 1.5T (GE LX 9.1, Waukesha, WI or Siemens Espree, Erlangan, Germany) with a multisequence MRI for measuring IMT and CINE MRI for measuring cyclic strain. Of those 30 subjects, all were healthy controls with no history of neurological or cardiovascular disease except seven patients with a known diagnosis of atherosclerosis and a history of stroke and/or heart attack. Informed consent was obtained in all subjects in this group under Huntington Hospital IRB protocol. The second groups of subjects (n=20, ages 18-78, 9 males, 11 females) were examined at 3.0T (Siemens Trio, Erlangan, Germany) using DENSE-MRI for an alternate means of measuring cyclic strain. Informed consent was obtained in all in this group under California Institute of Technology IRB protocol. There was no overlap in subjects between these two groups.

The imaging protocol for the 1.5T group consisted of the following: First, the patient was placed in the scanner supine and bilateral phased array carotid coils (GE: Medical Advances, Waukesha, WI; Siemens: Machnet, Netherlands) were placed at each side of the neck. Second, after the subject enters the scanner, a localizer image was acquired to ensure positioning of the carotid coils. Third, a time-of-flight magnetic resonance angiography (TOF MRA) was acquired and maximum intensity projections (MIP) were used to localize the carotid arteries. Finally, multiple slices perpendicular to the carotid arteries (axial) were acquired using 1) T1-weighted MRI, 2) T2-weighted MRI, 3) proton density-weighted MRI, 4) CINE MRI. The slices were centered at the bifurcation of the carotid artery as a landmark as shown in figure 4.1a. In this study, only the slices at the common carotid artery were utilized. This multisequence carotid imaging protocol was based on the parameters utilized in the national clinical trial of Multiethnic Study of Atherosclerosis [34, 35]. Table 4.1 describes the details of the

protocol acquired on the GE system and Table 3.2 for the Siemens system. Although the two manufacturers use different terminology to describe their pulse sequences and slightly different imaging parameters, the images produced were similar. At the time of the exam, all images were examined for the presence of atherosclerotic plaque by comparing the intensity of the lumen to the sternomastoid muscle in each of the different weighted scans. Table 4.3 describes the basic algorithm for MR characterization of atherosclerotic plaque. Total exam time was 30 minutes.

Table 4.1. GE LX 9.1 Sequence parameters

	2D Time of Flight	Black-blood Proton Density /T_2-weighted*	Black-blood T_1-weighted	CINE
Pulse sequence	3D spoiled GRE	2D FSE	2D FSE	FIESTA
TR (ms)	23	3500	500	9.93
TE (ms)	3.8	20/40	9.3	2.5
Flip angle	60	25	25	45
FOV (cm)	16x12	12x12	12x12	26x26
Matrix	256x128	256x192	256x192	160x160
Slice thickness (mm)	1	2	2	5
NEX	1	1	1	3
No. of slices	48	5	5	1
Special parameters	ETL=8, Fat sup	Fat sup	IT=600 ms, Fat sup	IT=600 ms, Fat sup, ECG

* GE uses a dual-echo pulse sequence to acquire proton density and T2-weighted images which are interleaved in reconstruction. Key: TR= Repetition Time, TE= Echo Time, FOV= Field Of View, NEX= Number of EXcitations, GRE= GRadient Echo, FSE= Fast Spin Echo, FIESTA= Fast Imaging Employing Steady sTate Acquisition (equivalent to steady-state free precession), ETL= Echo Train Length, Fat sup= Fat suppression, IT= inverstion time.

Table 4.2: Siemens Espree Sequence Parameters

	3D Time of Flight	Coronal T_2-weighted*	Black-blood Proton Density	Black-blood T_1-weighted	CINE
Pulse sequence	FLASH	3D TSE	2D TSE	2D TSE	2D FLASH
TR (ms)	31	1300	700	500	65.4
TE (ms)	7.15	143	10	9.3	4.3
Flip angle	60	n/a	180	180	15
FOV (cm)	20x15	19x14	14x14	14x14	15x12.5
Matrix	250x242	256x256	256x256	256x256	192x154
Slice thickness (mm)	1	0.74	2	2	4
NEX	1	2	1	1	3
No. of slices	40	72	5	5	3
Special parameters	Multislab	GRAPPAx2, Fat sup	DIR	DIR	DIR, ECG
Scan time	6:41	6:16	1:45	1:45	2:04

*Acquired as a 3D slab, data was then reconstructed to match the same slice locations as proton density and T1-weighted slices. Key: FLASH= Fast Low Angle Shot, TSE= Turbo-Spin Echo, GRAPPA= GeneRalized Autocalibrating Partially Parallel Acquisition, DIR=Double Inversion Recovery, aka dark-blood.

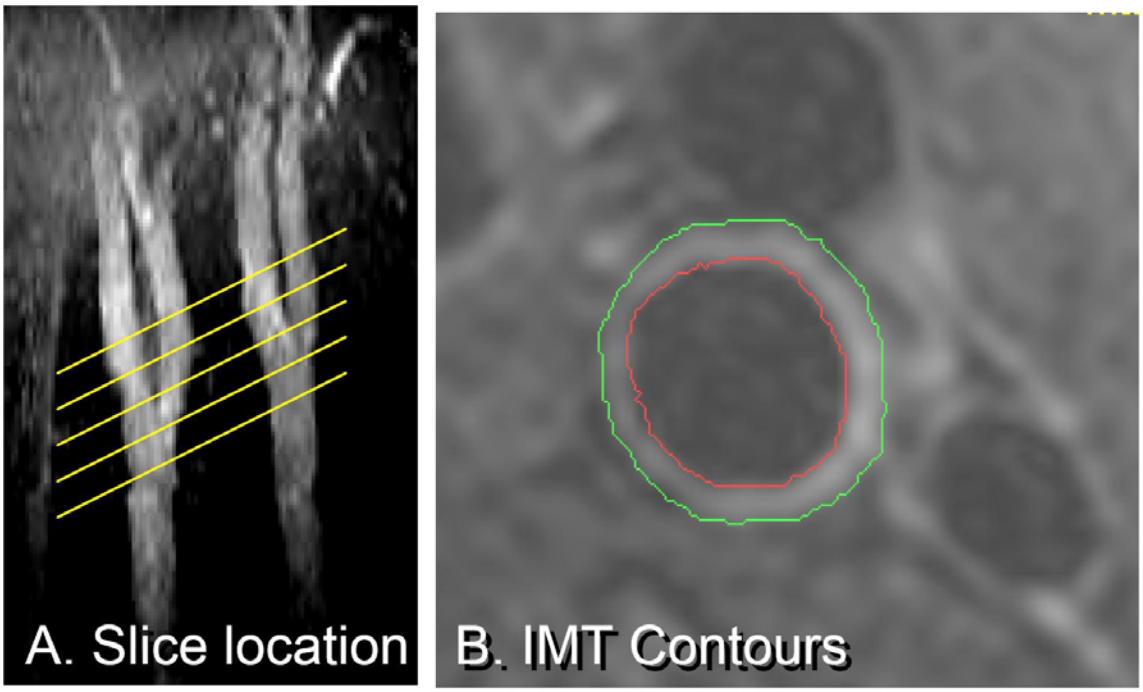

Figure 4.1. A) Slice location B) IMT contours.

Table 4.3. Plaque composition based on image contrast

	TOF	T_1W	PDW	T_2W
Plaque	+	+	+	+
Calcification	-	-	-	-
Hemorrhage	+	+	0	0
Fibrous matrix	0	0	+	0

Key: + = hyperintense, - = hypointense, 0 = isointense; intensity is compared to the sternomastoid muscle.

After the exam, all subject scans were transferred to a stand-alone workstation (GE Advanced Workstation). IMT measurements were calculated using Mass Analysis 6 which provides semiautomated segmentation of the carotid images and contours of the lumen wall as shown in Figure 4.1b. Contour registration was checked to ensure accurate segmentation of the lumen. In most cases, T_1-weighted images provided high-quality images from which the lumen wall thickness could be calculated. In some cases, patient motion, usually due to swallowing, may have affected the quality of the T_1w image in which case T_2w or proton density images were used for IMT thickness measurements. IMT thickness was calculated by taking the average of the lumen thickness across the entire lumen wall. In order to ensure axisymmetry and accuracy of this measurement, only the side which had the higher SNR and greatest circularity of the lumen area was selected. This same side was then used for cyclic strain measurement. Cyclic strain (ε_{CS}) was measured using the CINE MRI sequence where the systolic and diastolic lumen diameters were selected based on the maximum and minimum lumen areas, respectively. Cyclic strain was then calculated using the difference in systolic and diastolic lumen diameters divided by the diastolic diameter as described in the literature [14, 36, 37]. Age and body-mass index (BMI) were tabulated for each IMT and ε_{CS} measurement. Statistical analysis included two-tailed Pearson product moment correlation (with alpha values of 0.1, 0.4, 0.02, and 0.01) between IMT and strain to each other, BMI, and age

across controls and subjects with atherosclerosis. Due to the smaller sample size of the group with atherosclerosis, Wilcoxon ranked sum two sample test were used to determine significant differences between the controls and disease groups were conducted across all categories (age, BMI, IMT, and strain).

In the second group of subjects imaged at 3.0T, only a single-sided surface coil was available for imaging (Nova Medical, Wilmington, MA). The coil was placed on the side of the neck and secured with vacuum fixation pillow (Vacfix, S&S Par Scientific, Inc. Houston, TX). First, a rapid 3-plane true-FISP localizer was used to localize the coil and ensure proper placement of the coil relative to the carotid arteries. Second, an 3D multislab time-of-flight (TOF) MRI was acquired to localize the left or right carotid arteries and identify the bifurcation using maximum intensity projections (MIP) in sagittal and coronal views. Third, CINE MRI was acquired using 2D FLASH with TR=40ms and TE=3.4ms. Three 4 mm thick slices were prescribed on the MIP reconstructed images that were perpendicular to the common carotid artery, centered at the bifurcation, and spaced 9 mm apart. In this study only the slice at the common carotid artery is considered. In addition, in 16 of the 20 cases, blood pressure was taken at the time of the exam. Total exam time was 40 minutes.

In this group, circumferential strain is measured using the DENSE-MRI sequence. Details of the pulse sequence and postprocessing methods are described in detail in [28] however in short, DENSE images of the carotid artery wall were acquired at 0.6 * 0.6 * 4.0 mm^3 resolution, including displacement encoding in three oblique directions to produce a pixel-by-pixel 3D displacement map of the vessel wall and surrounding tissue. Image acquisition was consistently placed at the time of maximum lumen diameter, while the encoding portion was placed at 40 ms after the R-wave to capture the maximum wall

strain. From the displacement map, circumferential strain is calculated by measuring the deformation of the wall at quadrilateral points and averaging per pixel strain across the entire lumen wall. It is important to note that DENSE-MRI provides localized measures of strain that is not available in any other MR imaging technique however in this study only the mean strain across the entire lumen is used to provide a measure of cyclic strain that is comparable to the CINE cyclic strain measurements acquired at 1.5T. The relationship between circumferential strain and cyclic strain is defined in equation (4.2). Stiffness index was calculated as previously described [37] as defined in equation (4.3).

Results

Healthy Controls

In the control group at 1.5T, IMT ranged from 0.73mm to 2.12mm with a mean of 1.23mm $\pm$ 0.38 across the entire group. This fits well with previously published range of 0.8 to 1.8mm [9]. These results differ from ultrasound measurements (~0.8mm) where only parts of the lumen wall are visible to the method. MRI measurements are sensitive to the entire lumen wall including the adventitia which may provide better detection of focal thickening due to atherosclerosis [10]. These results are, to this date, the largest group of subjects in which CCA IMT is measured using MRI. IMT also shows a positive correlation with age ($r = 0.50$ with a significance of $p < 0.02$) as shown in Figure 4.2. There was no correlation with BMI as is shown in the size of the bubbles for each data point in the graph where the width of the data point is based on the BMI for that subject. There was not a statistical difference between males and females. These results confirm previously published results showing that IMT thickens with age as atherosclerosis is an ongoing process.

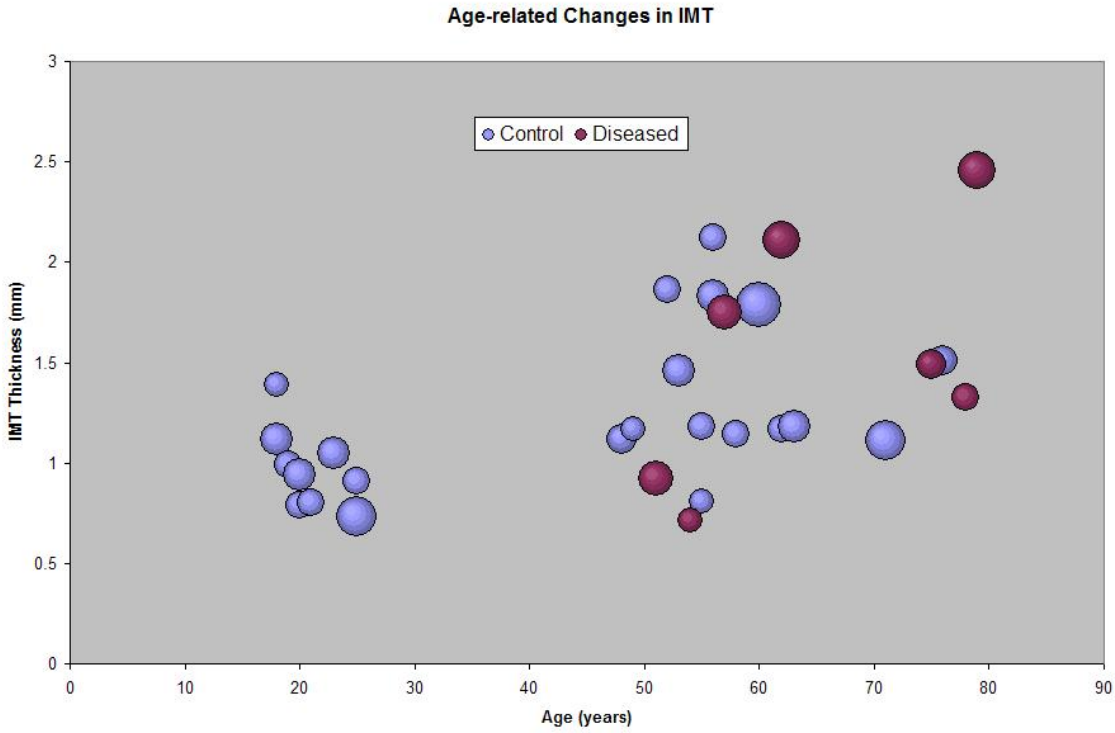

Figure 4.2. Correlation of IMT and age. The blue circles represent healthy controls, the purple circles represent those subjects with known atherosclerosis. BMI is proportional to the size of the data point.

It is expected that cyclic strain will decrease with age due to the well-documented increased stiffness of the carotid arteries with age. There was a strong correlation of ε_{CS} to age in the control group at 1.5T which confirms the hypothesis ($r = -0.55$ with a significance of $p < 0.01$) as shown in figure 4.3. Also shown in this figure by the size of the data points is that there was not a significant correlation between ε_{CS} and BMI. There also was not a significant difference in ε_{CS} between sexes.

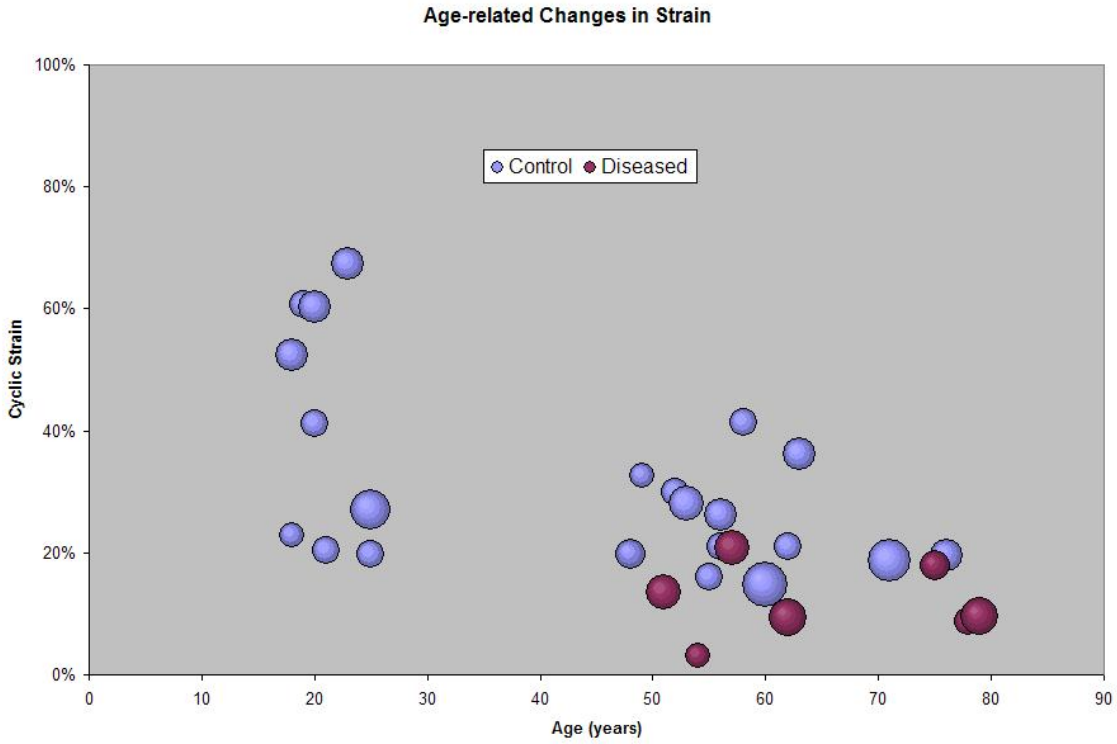

Figure 4.3. Correlation of strain and age. The blue circles represent healthy controls, the purple circles represent those subjects with known atherosclerosis. BMI is proportional to the size of the data point.

Mean ε_{CS} was 31.0% $\pm$ 15.7% with a range of 14.8% to 67.4%. This value is greater than the previous studies of 15% $\pm$ 5% using MRI and 18% $\pm$ 5% using ultrasound in [11] and 21% $\pm$ 9% and 18% $\pm$ 4% using MRI and ultrasound, respectively [38]. This is likely due to differences in the subject age populations as the measures of high ε_{CS} belong exclusively within the younger control population. The wide range of ε_{CS} values in the younger population is a unique observation that has not been previously published. Previous studies measuring cyclic strain generally focused on older populations. Based on the lack of correlation with BMI within this younger age group as shown in Figure 4.3, is there a relationship between IMT and strain? Statistically there is no correlation between IMT and strain. However, figure 4.4 shows that some of the young controls are characterized both by low strain and high IMT. This suggests that the

decreased strain may have clinical implications given the amount of evidence that supports the relation of IMT and risk of stroke.

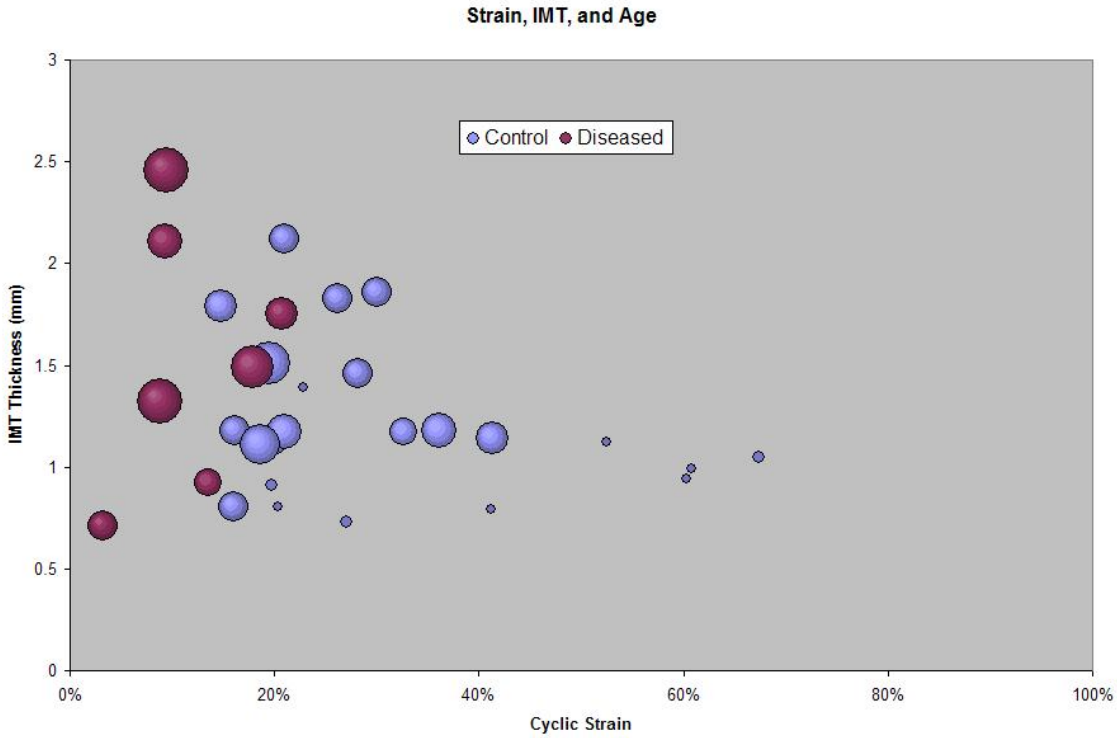

Figure 4.4. Correlation of cyclic strain with IMT and age. The blue circles represent healthy controls, the purple circles represent those subjects with known atherosclerosis. Age is proportional to the size of the data point.

Atherosclerosis

Multisequence MRI was effective at identifying plaque in the seven subjects with known atherosclerosis. It was also effective at ruling out atherosclerosis in the 23 healthy subjects. Figure 4.5 shows representative images that demonstrate plaque localization using the different contrasts of the imaging sequences. In four of the subjects, plaque was found lining the walls of the common carotid artery which accounts for higher IMT measurements in those subjects however there was no correlation between IMT and strain measurements. There was a statistically significant correlation ($r = 0.67$, $p < 0.10$) between IMT and BMI in this small sample size however there was no correlation with

age. There was also no correlation between cyclic strain and age, BMI, or CCA IMT. Using Wilcoxon two-sample test as well as heterodiastic two-tailed student t-test, CCA cyclic strain is significantly lower ($p<0.005$) in the atherosclerotic group when compared to the age and BMI matched controls (both student t-test and Wilcoxon tests showed that there were no significant difference in age and BMI between the two groups). IMT was not statistically different between these two groups. Details of the results in each of these subjects are described in Table 4.4 as well as statistics for age and weight-matched healthy controls.

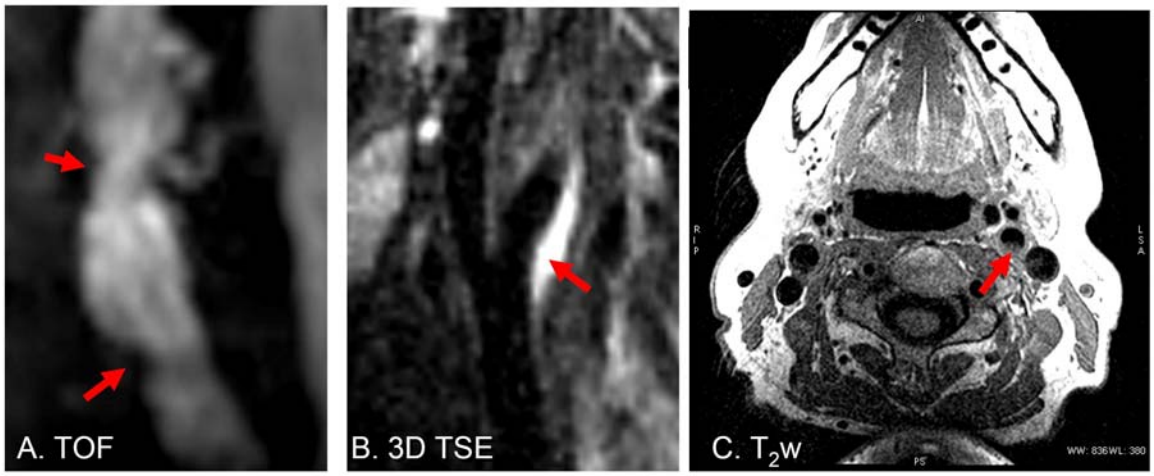

Figure 4.5 Multicontrast MRI of atherosclerosis at 1.5T

Table 4.4. Demographics and measurements in subjects with known atherosclerosis.

Subject	*Sex*	*Age (years)*	*BMI (kg/m^2)*	*IMT (mm)*	*ε_{CS} (%)*	*History*	*Plaque location*
A	M	51	27	0.92	13.5	Asymptomatic	ICA
B	F	54	20	0.71	3.2	Stroke	Bifurcation
C	F	57	26	1.75	20.8	Endarectomy	CCA
D	M	62	29	2.11	9.3	Stroke	CCA, bifurcation
E	F	75	22	1.49	17.8	Stroke	ICA
F	F	78	21	1.33	8.8	Stroke	CCA
G	M	79	28	2.46	9.5	Endarectomy	CCA, ICA
Mean	3M,4F	65±12	25±4	1.54 ±0.62	**24.1 +8.4**		
Control	6M,6F	60±7	24±4	1.43 ±0.40	**11.8 +6.0**		

Key: BMI= Body Mass Index, IMT= Intima-Media Thickness, ε_{CS} = cyclic strain, M= Male, F= Female, ICA= Internal Carotid Artery, CCA= common carotid artery

The significant difference in strain but not IMT is evident in figures 4.2 and 4.3 where wall thickness in subjects with atherosclerosis occupied the range of IMT found in normal controls whereas strain values were largely weighted towards the lower strain values, thus resulting in a statistically significant difference. Although the sample size of subjects with atherosclerosis is small, these results suggest that cyclic strain may be more diagnostic than IMT for atherosclerosis. It demonstrates that cyclic strain provides added value to the characterization of vessel wall using MRI.

DENSE-MRI Strain

Mean circumferential strain calculated by DENSE-MRI was 0.067 ± 0.030 which is in close agreement to previously published values of 0.071 ± 0.031 [28]. An example of a DENSE data set is shown in Figure 4.6. As with cyclic strain

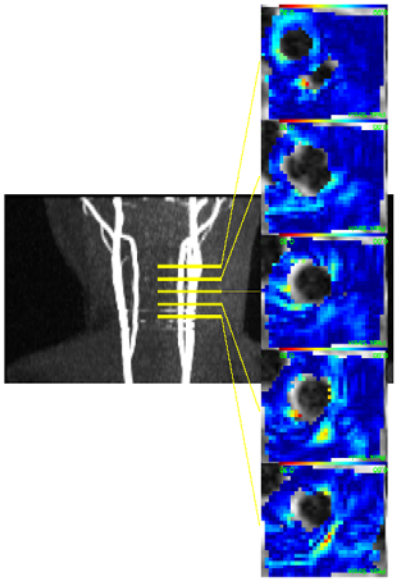

Figure 4.7 Representative DENSE data set. Note that although multiple slices can be acquired, in this study only a single slice from the common carotid was used.

measurements, there is a strong correlation of circumferential strain with age ($r = -0.64$, $p<0.01$) as shown in figure 4.7. The mean age of this group was 39.2 ± 20.9 with a BMI of 22.4 ± 4.2. There was no correlation of strain with BMI. Although this group is different from the 1.5T group in demographics, a similar pattern emerges where a broad range of strain values is found in the young, supposedly healthy individuals. This confirms the previous finding of this phenomenon in strain measurements.

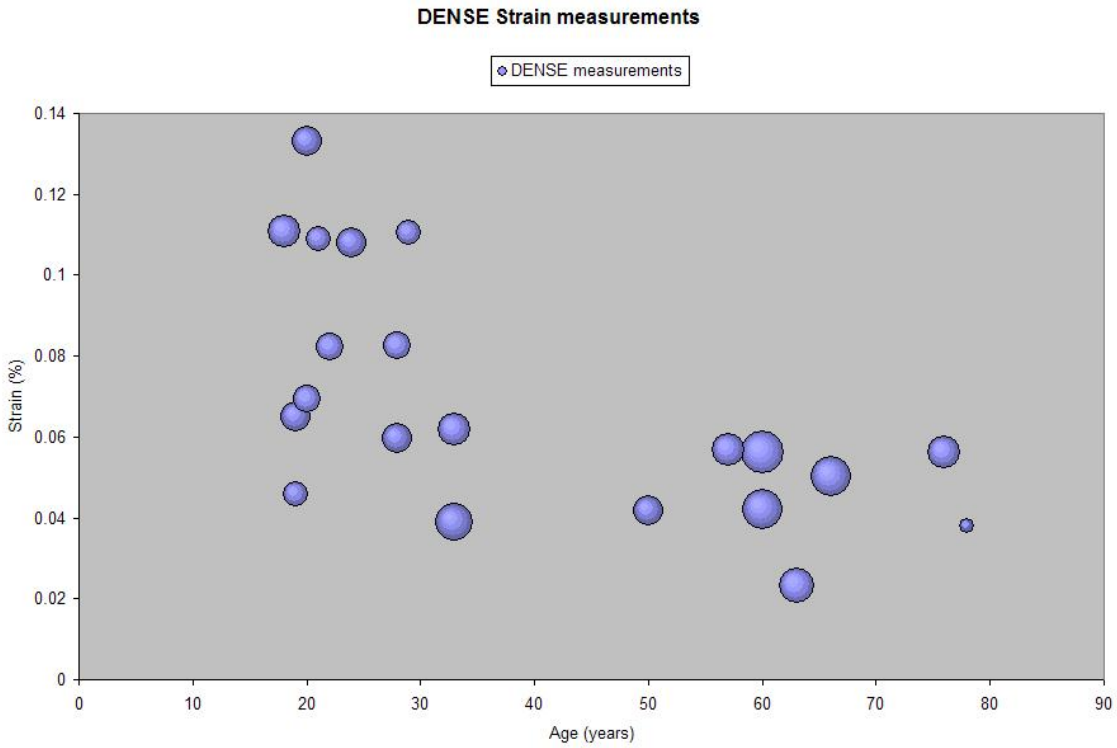

Figure 4.7. Correlation of DENSE strain with BMI and age. All data points are in normal, healthy subjects. BMI is proportional to the size of the data point.

In a subset of this group ($n = 16$) blood pressure measurements were obtained immediately after the DENSE-MRI data acquisition with the subject in the same position. Mean blood pressure in this group was $121/75 \pm 21/12$ which implies that subjects were normatensive. The stiffness index was calculated from circumferential strain and blood pressure differential and therefore showed correlation with both of those measures:

r = –0.66 ($p < 0.01$) and r = 0.55 ($p<0.01$) for stiffness index correlation with strain and blood pressure, respectively but did not show a correlation with age or BMI as shown in Figure 4.8. The mean stiffness index in this population was 4.6 $\pm$ 2.3 which is in the same range as previously published values of 5.6 $\pm$ 1.9 [33]. It was expected that the stiffness index would increase with age. However, these results do not confirm that hypothesis. This measurement has always of been some controversy due to the assumption that pressure at the brachial artery would be the same at the carotid [39].

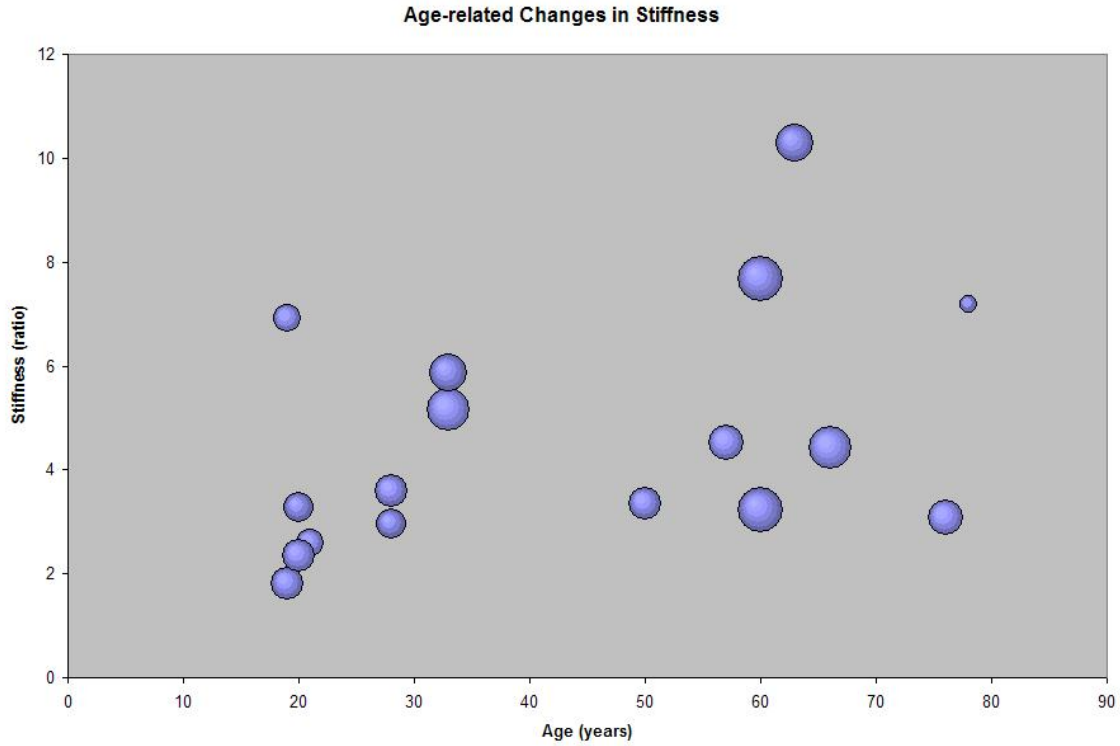

Figure 4.8. Correlation of stiffness with BMI and age. The blue circles represent healthy controls, the purple circles represent those subjects with known atherosclerosis. BMI is proportional to the size of the data point.

Discussion

This study presents a complete MRI protocol that can fully characterize the morphological and mechanical aspects of the common carotid arteries using quantitative

and noninvasive measurements of IMT and strain. A discussion of findings with each of these measures follows.

Multisequence MRI was useful in identifying atherosclerotic plaque in patients and for excluding the presence of plaque in the control group. It should be noted that the 3D sequences: 3D TOF MRA and most importantly the 3D-TSE sequence were the most valuable in excluding plaque. It is possible that smaller plaques might have been missed using multislice sequences whereas the 3D sequences allow for postacquisition reconstruction in multiple planes that can ensure that all aspects of the carotid vasculature can be visualized. It is also important to note that the quality of these images was dependent on the use of phased array carotid coils which offered enough signal to noise to adequately identify plaque and its components. This was one of the reasons why plaque detection was not attempted at 3T where phased array coils were not available at the time of the study. The commercial availability of 3T phased array coils will allow for the complete protocol to be acquired at the higher field strength which will provide higher-resolution images for better characterization of plaque.

The results of the IMT study confirmed the findings from ultrasound that show that the common carotid artery thickens with age. However, IMT thickness did not differentiate patients with atherosclerotic plaque from healthy, age-matched controls. Previous MRI studies of IMT were either conducted solely in normal controls [10, 11] or solely in patient populations [9, 40]. While one study [40] concludes that patients with an IMT thickness greater than 1.2 mm showed significantly higher plaque load, normal controls were not examined. The results of this study show that normal, healthy controls can exhibit high IMT thickness as well. Therefore, future studies with IMT measurements must take into account normal range of IMT and its age dependency.

Unlike IMT, cyclic strain in the common carotid artery showed significant differences between the patient and control populations. Although a previous study showed a significant difference between control and hypertensive patients [11], changes in cyclic strain as measured by MRI in atherosclerotic patients is a unique observation. These results confirm ultrasound findings that cyclic strain is decreased in atherosclerosis and confirm biological [41] and biomechanical models [42] that have long predicted such an outcome. Furthermore, the correlation between strain and age also confirms previous ultrasound studies and provides a normative database from which future comparisons can be made. These results form the basis for a more careful examination of strain in the carotid arteries which can be achieved with DENSE-MRI.

It is important to note that the application of DENSE-MRI in this study was limited to measuring average strain around the lumen wall. The unique value of DENSE-MRI lies in its ability to characterize strain in any portion of the lumen wall. Currently, the only other available technique for similar measurements is the use of intravascular ultrasound [43], an invasive technique that suffers from the same problems of user variability in ultrasound measurements [44, 45]. Due to limitations of the IRB protocol, DENSE-MRI could not be applied to patients, however future studies of atherosclerosis in the carotid arteries will include this method. Given the results of this study which show that strain plays a significant role in carotid atherosclerosis, DENSE-MRI would carry these observations further by characterizing strain in the plaque itself. This would provide insight into the plaque vulnerability, one of the biggest clinical questions that surround the diagnosis of atherosclerosis.

References

1. Myerburg, R. J., Interian, A., Jr., Mitrani, R. M., Kessler, K. M., Castellanos, A., Frequency of sudden cardiac death and profiles of risk. *Am J Cardiol* **1997,** 80(5B), 10F–19F.
2. Agabiti-Rosei, E., Muiesan, M. L., Carotid atherosclerosis, arterial stiffness and stroke events. *Adv Cardiol* **2007,** 44, 173–186.
3. De Groot, E., van Leuven, S. I., Duivenvoorden, R., Meuwese, M. C., Akdim, F., Bots, M. L., Kastelein, J. J., Measurement of carotid intima-media thickness to assess progression and regression of atherosclerosis. *Nat Clin Pract Cardiovasc Med* **2008,** 5(5), 280–288.
4. Bots, M. L., Hoes, A. W., Koudstaal, P. J., Hofman, A., Grobbee, D. E., Common carotid intima-media thickness and risk of stroke and myocardial infarction: the Rotterdam Study. *Circulation* **1997,** 96(5), 1432–1437.
5. Hollander, M., Bots, M. L., Del Sol, A. I., Koudstaal, P. J., Witteman, J. C., Grobbee, D. E., Hofman, A., Breteler, M. M., Carotid plaques increase the risk of stroke and subtypes of cerebral infarction in asymptomatic elderly: the Rotterdam study. *Circulation* **2002,** 105(24), 2872–2877.
6. Chambless, L. E., Heiss, G., Folsom, A. R., Rosamond, W., Szklo, M., Sharrett, A. R., Clegg, L. X., Association of coronary heart disease incidence with carotid arterial wall thickness and major risk factors: the Atherosclerosis Risk in Communities (ARIC) Study, 1987-1993. *Am J Epidemiol* **1997,** 146(6), 483–494.
7. Heiss, G., Sharrett, A. R., Barnes, R., Chambless, L. E., Szklo, M., Alzola, C., Carotid atherosclerosis measured by B-mode ultrasound in populations:

associations with cardiovascular risk factors in the ARIC study. *Am J Epidemiol* **1991,** 134(3), 250–256.

8. De Groot, E., Zwinderman, A. H., van der Steen, A. F., Ackerstaff, R. G., Montauban van Swijndregt, A. D., Bom, N., Lie, K. I., Bruschke, A. V., Variance components analysis of carotid and femoral intima-media thickness measurements. REGRESS Study Group, Interuniversity Cardiology Institute of The Netherlands, Utrecht, The Netherlands. Regression Growth Evaluation Statin Study. *Ultrasound Med Biol* **1998,** 24(6), 825–832.
9. Underhill, H. R., Kerwin, W. S., Hatsukami, T. S., Yuan, C., Automated measurement of mean wall thickness in the common carotid artery by MRI: a comparison to intima-media thickness by B-mode ultrasound. *J Magn Reson Imaging* **2006,** 24(2), 379–387.
10. Boussel, L., Serusclat, A., Skilton, M. R., Vincent, F., Bernard, S., Moulin, P., Saloner, D., Douek, P. C., The reliability of high resolution MRI in the measurement of early stage carotid wall thickening. *J Cardiovasc Magn Reson* **2007,** 9(5), 771–776.
11. Crowe, L. A., Ariff, B., Keegan, J., Mohiaddin, R. H., Yang, G. Z., Hughes, A. D., Mc, G. T. S. A., Firmin, D. N., Comparison between three-dimensional volume-selective turbo spin-echo imaging and two-dimensional ultrasound for assessing carotid artery structure and function. *J Magn Reson Imaging* **2005,** 21(3), 282–289.
12. Shinnar, M., Fallon, J. T., Wehrli, S., Levin, M., Dalmacy, D., Fayad, Z. A., Badimon, J. J., Harrington, M., Harrington, E., Fuster, V., The diagnostic

accuracy of ex vivo MRI for human atherosclerotic plaque characterization. *Arterioscler Thromb Vasc Biol* **1999,** 19(11), 2756–2761.

13. Yuan, C., Mitsumori, L. M., Beach, K. W., Maravilla, K. R., Carotid atherosclerotic plaque: noninvasive MR characterization and identification of vulnerable lesions. *Radiology* **2001,** 221(2), 285–299.

14. Younis, H. F., Kaazempur-Mofrad, M. R., Chan, R. C., Isasi, A. G., Hinton, D. P., Chau, A. H., Kim, L. A., Kamm, R. D., Hemodynamics and wall mechanics in human carotid bifurcation and its consequences for atherogenesis: investigation of inter-individual variation. *Biomech Model Mechanobiol* **2004,** 3(1), 17–32.

15. Dijk, J. M., van der Graaf, Y., Grobbee, D. E., Bots, M. L., Carotid stiffness indicates risk of ischemic stroke and TIA in patients with internal carotid artery stenosis: the SMART study. *Stroke* **2004,** 35(10), 2258–2262.

16. Safar, M. E., Blacher, J., Mourad, J. J., London, G. M., Stiffness of carotid artery wall material and blood pressure in humans: application to antihypertensive therapy and stroke prevention. *Stroke* **2000,** 31(3), 782–790.

17. Laurent, S., Boutouyrie, P., Arterial stiffness and stroke in hypertension: therapeutic implications for stroke prevention. *CNS Drugs* **2005,** 19(1), 1–11.

18. Simons, P. C., Algra, A., Bots, M. L., Grobbee, D. E., van der Graaf, Y., Common carotid intima-media thickness and arterial stiffness: indicators of cardiovascular risk in high-risk patients. The SMART Study (Second Manifestations of ARTerial disease). *Circulation* **1999,** 100(9), 951–957.

19. Van Popele, N. M., Grobbee, D. E., Bots, M. L., Asmar, R., Topouchian, J., Reneman, R. S., Hoeks, A. P., van der Kuip, D. A., Hofman, A., Witteman, J. C.,

Association between arterial stiffness and atherosclerosis: the Rotterdam Study. *Stroke* **2001,** 32(2), 454-60.

20. Roman, M. J., Devereux, R. B., Schwartz, J. E., Lockshin, M. D., Paget, S. A., Davis, A., Crow, M. K., Sammaritano, L., Levine, D. M., Shankar, B. A., et al., Arterial stiffness in chronic inflammatory diseases. *Hypertension* **2005,** 46(1), 194–199.

21. Scuteri, A., Brancati, A. M., Gianni, W., Assisi, A., Volpe, M., Arterial stiffness is an independent risk factor for cognitive impairment in the elderly: a pilot study. *J Hypertens* **2005,** 23(6), 1211–1216.

22. Van de Putte, E. M., Uiterwaal, C. S., Bots, M. L., Kuis, W., Kimpen, J. L., Engelbert, R. H., Is chronic fatigue syndrome a connective tissue disorder? A cross-sectional study in adolescents. *Pediatrics* **2005,** 115(4), e415–422.

23. Benetos, A., Waeber, B., Izzo, J., Mitchell, G., Resnick, L., Asmar, R., Safar, M., Influence of age, risk factors, and cardiovascular and renal disease on arterial stiffness: clinical applications. *Am J Hypertens* **2002,** 15(12), 1101–1108.

24. Matsui, Y., Kario, K., Ishikawa, J., Eguchi, K., Hoshide, S., Shimada, K., Reproducibility of arterial stiffness indices (pulse wave velocity and augmentation index) simultaneously assessed by automated pulse wave analysis and their associated risk factors in essential hypertensive patients. *Hypertens Res* **2004,** 27(11), 851–857.

25. Millasseau, S. C., Stewart, A. D., Patel, S. J., Redwood, S. R., Chowienczyk, P. J., Evaluation of carotid-femoral pulse wave velocity: influence of timing algorithm and heart rate. *Hypertension* **2005,** 45(2), 222–226.

26. Aletras, A. H., Ding, S., Balaban, R. S., Wen, H., DENSE: displacement encoding with stimulated echoes in cardiac functional MRI. *J Magn Reson* **1999,** 137(1), 247–252.

27. Wen, H., Vignaud, A., Rodriquez, I., Regional strain mapping of the carotid artery wall in Humans using DENSE. *Magn Reson Mater Phy* **2005,** 18(S1), S60–S61.

28. Lin, A. P., Bennett, E., Wisk, L., Gharib, M., Fraser, S., Wen, H., Circumferential Strain in the Wall of the Common Carotid Artery: Comparing Displacement-Encoded and CINE MRI in Volunteers. *Magn Reson Med* **2008,** 60(1), 8–13.

29. Lin, A. P., Bennett, E., Wisk, L., Gharib, M., Fraser, S., Wen, H. Mapping 2D Strain in the Wall of the Carotid Artery Using Displacement-Encoded MRI., In *Proceedings of International Society of Magnetic Resonance in Medicine,* Berlin, Germany, 2007.

30. Lin, A. P., Tyszka, J. M., Bennett, E., Fraser, S., Wen, H., Preliminary Validation of Circumferential Strain Measurements using DENSE at 1.5T and 3T. *J Cardiovasc Magn Reson* **2006,** 8(1), 48–49.

31. Lusis, A. J., Atherosclerosis. *Nature* **2000,** 407(6801), 233–241.

32. Mitchell, G. F., Parise, H., Benjamin, E. J., Larson, M. G., Keyes, M. J., Vita, J. A., Vasan, R. S., Levy, D., Changes in arterial stiffness and wave reflection with advancing age in healthy men and women: the Framingham Heart Study. *Hypertension* **2004,** 43(6), 1239–1245.

33. Juonala, M., Kahonen, M., Laitinen, T., Hutri-Kahonen, N., Jokinen, E., Taittonen, L., Pietikainen, M., Helenius, H., Viikari, J. S., Raitakari, O. T., Effect of age and sex on carotid intima-media thickness, elasticity and brachial

endothelial function in healthy adults: the cardiovascular risk in Young Finns Study. *Eur Heart J* **2008,** 29(9), 1198–1206.

34. Hatsukami, T. S., Ross, R., Polissar, N. L., Yuan, C., Visualization of fibrous cap thickness and rupture in human atherosclerotic carotid plaque in vivo with high-resolution magnetic resonance imaging. *Circulation* **2000,** 102(9), 959–964.

35. Yuan, C., Kerwin, W. S., Yarnykh, V. L., Cai, J., Saam, T., Chu, B., Takaya, N., Ferguson, M. S., Underhill, H., Xu, D., et al., MRI of atherosclerosis in clinical trials. *NMR Biomed* **2006,** 19(6), 636–654.

36. Draney, M. T., Herfkens, R. J., Hughes, T. J., Pelc, N. J., Wedding, K. L., Zarins, C. K., Taylor, C. A., Quantification of vessel wall cyclic strain using cine phase contrast magnetic resonance imaging. *Ann Biomed Eng* **2002,** 30(8), 1033–1045.

37. Mackenzie, I. S., Wilkinson, I. B., Cockcroft, J. R., Assessment of arterial stiffness in clinical practice. *Qjm* **2002,** 95(2), 67–74.

38. Leeson, C. P., Robinson, M., Francis, J. M., Robson, M. D., Channon, K. M., Neubauer, S., Wiesmann, F., Cardiovascular magnetic resonance imaging for non-invasive assessment of vascular function: validation against ultrasound. *J Cardiovasc Magn Reson* **2006,** 8(2), 381–387.

39. Waddell, T. K., Dart, A. M., Medley, T. L., Cameron, J. D., Kingwell, B. A., Carotid pressure is a better predictor of coronary artery disease severity than brachial pressure. *Hypertension* **2001,** 38(4), 927–931.

40. Mani, V., Aguiar, S. H., Itskovich, V. V., Weinshelbaum, K. B., Postley, J. E., Wasenda, E. J., Aguinaldo, J. G., Samber, D. D., Fayad, Z. A., Carotid black blood MRI burden of atherosclerotic disease assessment correlates with

ultrasound intima-media thickness. *J Cardiovasc Magn Reson* **2006,** 8(3), 529–534.

41. Wung, B. S., Cheng, J. J., Hsieh, H. J., Shyy, Y. J., Wang, D. L., Cyclic strain-induced monocyte chemotactic protein-1 gene expression in endothelial cells involves reactive oxygen species activation of activator protein 1. *Circ Res* **1997,** 81(1), 1–7.

42. Fung, Y. C., *Biomechanics : mechanical properties of living tissues*. 2nd ed.; Springer-Verlag: New York, 1993; p xviii, pgs 568.

43. Schaar, J. A., De Korte, C. L., Mastik, F., Strijder, C., Pasterkamp, G., Boersma, E., Serruys, P. W., Van Der Steen, A. F., Characterizing vulnerable plaque features with intravascular elastography. *Circulation* **2003,** 108(21), 2636–2641.

44. De Korte, C. L., Cespedes, E. I., Van Der Steen, A. W., Influence of catheter position on estimated strain in intravascular elastography. *IEEE Trans Ultrason Ferroelectr Freq Control* **1999,** 46(3), 616–625.

45. Godia, E. C., Madhok, R., Pittman, J., Trocio, S., Ramas, R., Cabral, D., Sacco, R. L., Rundek, T., Carotid artery distensibility: a reliability study. *J Ultrasound Med* **2007,** 26(9), 1157–1165.

Chapter 5: Case Study

This study concludes with a case study that demonstrates the potential role that DENSE MRI may play in advanced stroke diagnosis. A 79-year-old male had a history of a left carotid atherosclerosis that resulted in a bilateral endarterectomy at age 60. This subject had a BMI of 28.1 and a history of smoking and cholesterol but blood pressure was normal and he had no history of diabetes, cardiovascular disease, or stroke. Duplex carotid ultrasound was performed one week prior to the MRI exam which demonstrated a restonosis of the left internal carotid artery with a peak systolic blood flow velocity of 370 cm/sec with an ICA/CCA ratio of 3.6 as compared to 134 cm/sec and 1.1, respectively on the right. The goal of the MRI scan was to image atherosclerotic plaque using multisequence MRI and to measure strain using DENSE-MRI.

Prior to the MRI exam, special care was taken to ensure that any remaining clips from the surgery were MR compatible at both 1.5T and 3.0T field strengths and subject consent was obtained at both 1.5T and 3.0T under Huntington Hospital and Caltech IRB protocols, respectively. At 1.5T, multisequence MRI comprised of a 3 plane fast gradient echo localizer, 3D time of flight magnetic resonance angiography (TOF-MRA), 5 slice axial proton density, T2-weighted (T2w), and T1-weighted (T1w) MRI centered at the bifurcation as previously described. In addition, 3D turbo spin echo (aka SPACE) MRI was acquired for 3D T2-weighted coverage of the entire carotid artery using a coronal slab and CINE MRI for a rough measure of strain was also acquired at the common carotid artery. The 3T exam was performed immediately following the 1.5T exam which consisted of a 3 plane localizer, 2D time of flight, axial CINE MRI, and 3 slice axial

single-shot DENSE MRI centered at the bifurcation where the top slice was 1 cm above at the internal (ICA) and external carotid arteries (ECA) and 1 cm below at the common carotid artery (CCA). Both 1.5T and 3.0T acquisition parameters were identical to those described in detail in the previous chapter. The multisequence MRI data was analyzed using QPlaque software which automatically coregisters all multisequence images such that T1w and PDw slices correspond anatomically with 3D TOF and SPACE images. The advantage of the coregistration is that it provides comparisons signal intensities across each slice in a single view. The images were then manually segmented based on tissue contrast to delineate lipid core, hemorrhage, and calcification as described in the literature. The software also provides semiautomated contouring that enabled rapid determination of IMT thickness. DENSE MRI was processed using DENSEview as previously described to obtain strain maps and circumferential strain measurements of the carotid arteries at the CCA, bifurcation, and ICA.

The results show that this MR imaging protocol provides a wealth of information that would be valuable to physicians in determining the care for this patient. A maximum intensity projection of the TOF MRA confirmed evidence of a high-grade stenosis at the left internal carotid artery approximately 1.8 cm above the bifurcation as indicated by the arrow in Figure 5.1a. The 3D TSE reconstruction also confirms this stenosis however it also shows atherosclerotic plaques at the carotid bulb and immediately above the bifurcation as indicated by the dotted arrows in Figure 5.1b which were not described by the initial duplex ultrasound exam. Current medical care standards would dictate that the high-grade stenosis would be re-operated on and removed however it is unclear whether

the surgeons would have acted on the atherosclerosis discovered at the carotid bulb and inferior portion of the ICA. Therefore these newer regions were of greater interest.

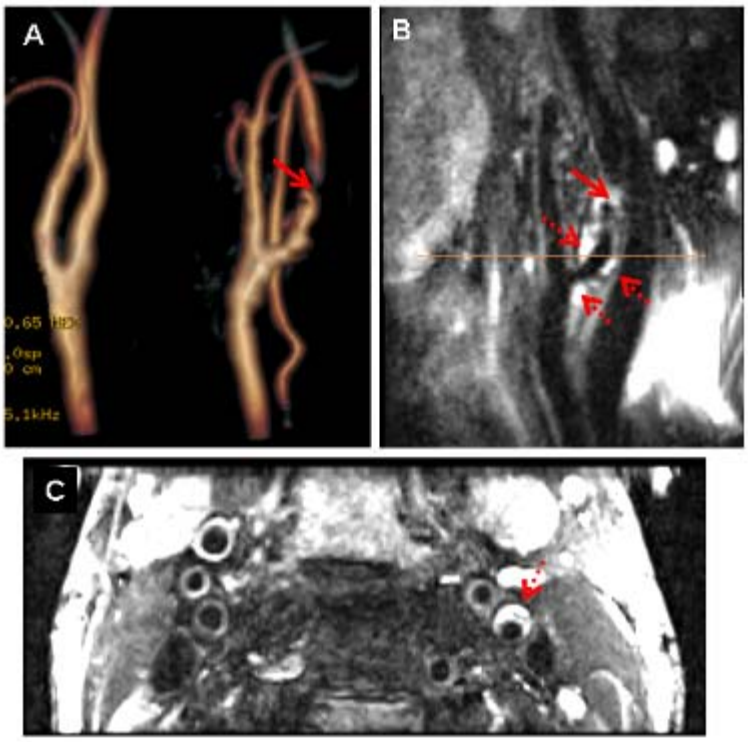

Figure 5.1. MRI of the carotid arteries.
A. Maximum intensity projection of the 3D time of flight magnetic resonance angiography acquired at 1.5T. The red arrow indicates stenosis due to plaque.
B. 3D TSE oblique reconstruction of the left carotid artery. The solid red arrow indicates the stenosis in Fig 1A. The dotted arrows indicate additional plaques.
C. 3D TSE axial reconstruction at the bifurcation. Slice location is indicated by the organe line in Fig 1B. Dotted arrow indicates plaque region.

An axial reconstruction of the 3D TSE data clearly shows the plaque in Figure 5.1c. Figure 5.2 shows the multisequence reconstruction using QPlaque in this same region with the semiautomated contouring of the intima and media of the carotid artery giving an IMT of 2.32 $\pm$ 0.86 mm, wall area of 45.4 mm^2, and lumen area of 13.1 mm^2. The yellow outline covers a region of 17.55 mm^2 that shows hyperintense signal when compared to the sternocleidomastoid muscle on all four sequences. Only the lipid core would show hyperintense signal in TOF, T1w, T2w, and PDw images. There is also a region of hypointense or null signal in the proton density image that likely corresponds to intimal calcification that is indicated in the shaded brown region. From these regions, QPlaque then calculates the fibrous cap thickness of 1.17 $\pm$ 0.17 mm.

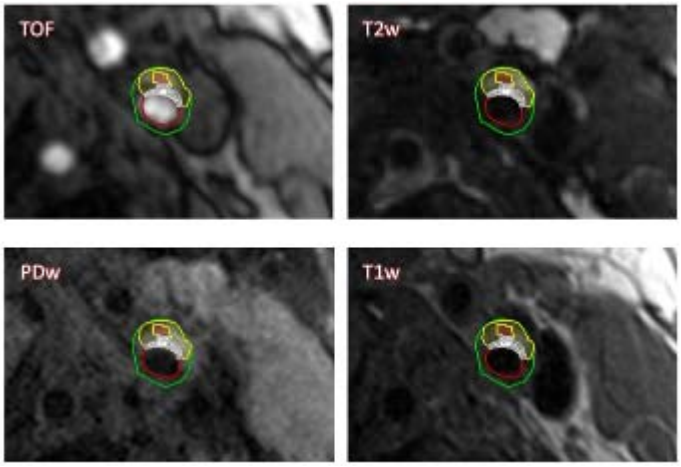

Figure 5.2. Multisequence MRI of the left carotid artery just above the bifurcation.
3D MIP of TOF MRA (top left) and corresponding sT1w, T2w, and PD slices. The yellow region marks the lipid core whereas the brown region marks calcification. The hash lines show the fibrous cap thickness.

The DENSE MRI data, shown in Figure 3, shows the first strain measurements in atherosclerotic plaque. The first observation is that at the common carotid artery, where there is no evidence of plaque, that uniformly low strain value is observed. This confirms results from the previous study in patients with a history of stroke that even nonaffected portions of the carotid artery provide abnormal strain measurements. The second observation is that strain in the carotid plaque at the bifurcation appears low. This corresponds with IVUS results that also demonstrate low strain in the plaque. It is interesting to note however that there appears to correspondingly higher strain in the lumen wall opposite of the plaque both at the bifurcation and at the ICA (note however the ICA slice is 0.7mm inferior to the high-grade stenosis observed in ultrasound). This nonuniformity of strain would not be observed by traditional ultrasound distension measurements. This additional biomechanical information could prove to be valuable in patient diagnostics however with a single case study it is difficult to draw any conclusions.

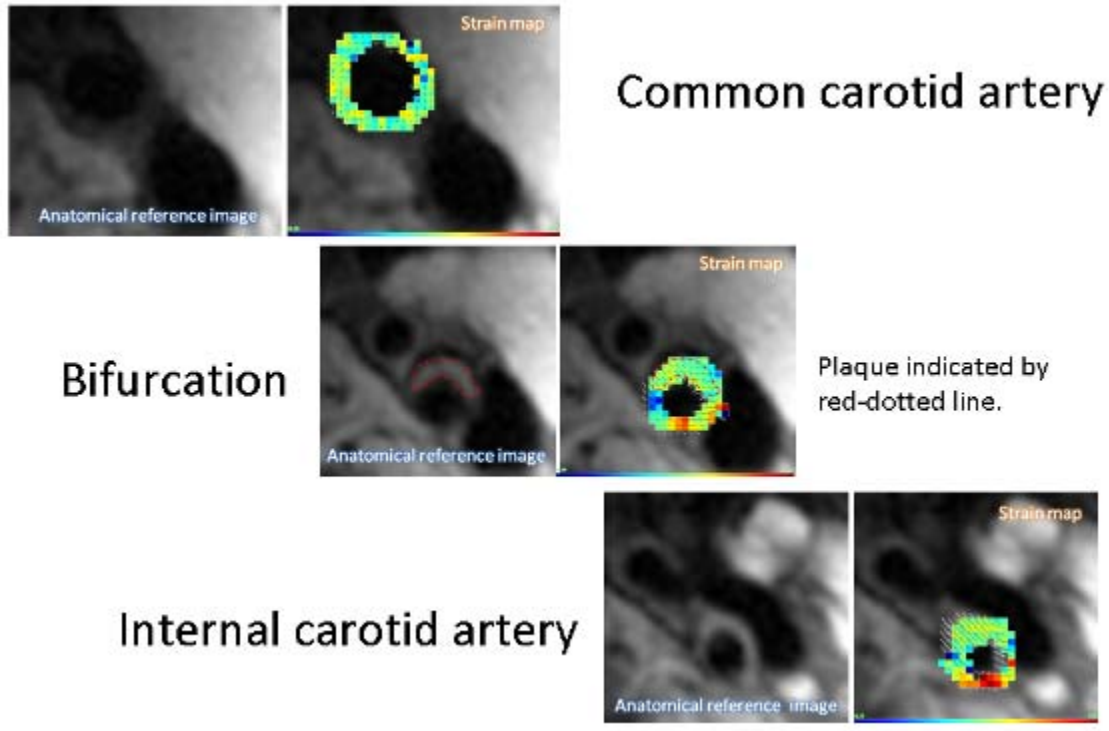

Figure 5.3. DENSE MRI strain maps and corresponding anatomical region at each acquired slice.

Based on the IVUS studies, plaque vulnerability is defined by a region of high strain in the fibrous cap of the atheroma. In this patient, this is not observed which indicates that this is likely a stable plaque. While this conclusion must be confirmed by larger patient studies, this type of information that can be obtained from the DENSE MRI data would be of value to surgeons. Had there been evidence of high strain, it would have been necessary to not only remove the plaque observed in the superior portion of the internal carotid artery but also at the bifurcation as well.

A follow-up CT angiogram was performed three weeks after the MRI exam. The results of the CT scan showed that the "left carotid bulb demonstrates mural atheromatous with mild narrowing" as well as evidence of calcification in the left carotid artery. These

results confirm the findings from the multisequence MRI and also show that MRI is sensitive to plaque that was missed in the duplex ultrasound exam. Furthermore, neither duplex ultrasound nor the subsequent CT exam can provide the functional information that DENSE MRI can provide on the vulnerability of the plaque. This case study demonstrates an ideal MR imaging protocol that provides high resolution morphological imaging as well as important functional strain mapping. Due to lack of research license at 1.5T and lack of clinical carotid imaging protocols at 3T, it was not possible to conduct those two protocols in a single exam however these issues are local issues that would be easily surmounted in a university hospital environment resulting in an exam that would take no longer than 45 minutes that would provide a "one-stop shop" for imaging atherosclerosis in the carotid arteries. This initial result underscores the need for future studies that can determine the efficacy of DENSE strain measurements combined with morphological information from multisequence MRI.

Chapter 6: Conclusion

Study Limitations

Although the results described in chapters 4 and 5 show significant changes in strain in subjects with thickened IMT and atherosclerosis, strain measurements alone do not paint a complete picture of the biomechanics of the carotid arteries. The stress-strain relationship is important for a thorough understanding of the material properties of the artery [1]. In this situation, stress is induced by luminal blood pressure. Ideally, blood pressure at the location of the DENSE strain measurements would be necessary to fully characterize the biomechanical state of the carotid artery. However, in order to accurately measure blood pressure at that specific point, a pressure catheter must be used which is a highly invasive procedure and would not be possible to be measured at the time of the DENSE-MRI. Some studies have shown that blood pressure can be mapped using phase-contrast MRI [2] however these measurements utilize Bernoulli equations using velocity encoded data. These calculations require broad assumptions of the nature of flow in the carotid artery. Finite element analysis based on the anatomy as well as the flow data would provide a much more accurate estimate of localized blood pressure [3] but was outside the scope of this thesis.

More conventional blood pressure measurements using a cuff manometer is another method of assessing stress in the carotid arteries. As described in chapter 4, some blood pressure measurements were taken at the time of the MRI exam but not during the DENSE MRI measurement. It is quite possible that the blood pressure changed during the DENSE MRI due to patient anxiety or relaxation. Furthermore, brachial measurements provide only a generalized estimate of systolic and diastolic blood pressure in the carotid artery and so this method would still be an indirect measurement

of blood pressure induced stress. Nonetheless, studies have shown a direct relationship between carotid artery stiffness and blood pressure [4]. Future studies could incorporate blood pressure measurements at the time of data acquisition using MR-compatible blood pressure monitors at the time of the exam.

Another biomechanical function that is not considered in this thesis is the effect of shear stress on the formation of atherosclerotic plaques. Numerous studies have shown the relationship between hemodynamics in the carotid arteries and atherogenesis [5-7]. It is also possible to measure shear stress using magnetic resonance imaging [8-10] however calculation of wall shear stress requires complex computational fluid dynamic modeling and simulation which was also outside the scope of this thesis. Future studies could utilize available MRI sequences to characterize this important feature of carotid biomechanics.

Future Studies

The primary contribution of this thesis was to develop a method for imaging strain noninvasively using DENSE-MRI in the carotid arteries. First, validation of the strain measurements obtained with DENSE-MRI was demonstrated in an *in vivo* study where quantitative measures of mean strain in the wall of the carotid artery showed excellent correlation with circumferential strain as measured by the change in the lumen area. The validation study also demonstrated high reproducibility of the data processing methods and showed variance around the lumen wall which prove that the assumption that strain is uniform throughout the carotid wall is not true and that localized measures of strain, provided by DENSE-MRI, would be necessary for the full biomechanical characterization of strain in the carotid arteries. The second study made improvements

on the DENSE-MRI sequence by using a single-shot implementation. Single-shot DENSE effectively removed imaging artifacts that would have caused inaccuracies in the strain measurements. This was an important achievement because it allowed for accurate strain measurements above the bifurcation where strain mapping would be most diagnostic for atherosclerosis. In addition, the use of rigid body registration of the single shot data reduced the errors from subject movement. This is critical step toward the implementation of DENSE-MRI in the medical clinic where subject movement can not be avoided. The final study incorporates strain mapping into a clinical carotid imaging protocol that defines the morphological characterization of the carotid arteries. The results of that study provides normative strain data from which future studies can be based. The ultimate goal of this research was to develop a clinically relevant diagnostic test for atherosclerosis in the carotid arteries. To that extent, a description of future studies is necessary to demonstrate the steps that need to be taken in order to translate the DENSE-MRI method to a clinically diagnostic tool.

The steps that would be required to demonstrate that DENSE-MRI strain measurements are clinically relevant would require the following two studies:

Study I: Patients with known atherosclerosis would be recruited and imaged with DENSE-MRI. Strain patterns in atherosclerotic plaques would be compared with nonaffected contralateral side in the same region of the carotid artery. Reproducibility and variability of these strain measurements would also be determined. The first hypothesis is that strain in patients will be significantly different in the plaques.

Study II: Correlation of strain measurements with morphological measures of atherosclerosis from structural MRI as well as clinical measures of atherosclerosis would be made. The second hypothesis is that DENSE-MRI strain measurements in the plaque

will correlate with increasing severity of atherosclerotic disease as determined by morphological and clinical measures.

If these two studies are completed and the hypotheses proven true, then there would exist well-documented evidence that DENSE-MRI strain is correlated with measures of atherosclerosis. Additional measurements as described in study limitations above would also help to better define the correlation. At this point a prospective study would be the next goal where DENSE-MRI strain measurements would be measured in patients. The patients would then be followed to determine if the strain measurements are predictive of outcome (i.e. plaque rupture). If this measure is established, DENSE-MRI would provide early diagnosis of stroke and predictive of plaque vulnerability with such efficacy that treatment can be provided before the devastating effects of the disease can take their course. This has been the long-term goal of this thesis work and I hope that I have inspired the reader of the worthiness of this goal.

References

1. Fung, Y. C., *Biomechanics : mechanical properties of living tissues*. 2nd ed.; Springer-Verlag: New York, 1993; 568 pgs.
2. Tyszka, J. M., Laidlaw, D. H., Asa, J. W., Silverman, J. M., Three-dimensional, time-resolved (4D) relative pressure mapping using magnetic resonance imaging. *J Magn Reson Imaging* **2000,** 12(2), 321–329.
3. Thubrikar, M. J., Robicsek, F., Pressure-induced arterial wall stress and atherosclerosis. *Ann Thorac Surg* **1995,** 59(6), 1594–1603.
4. Safar, M. E., Blacher, J., Mourad, J. J., London, G. M., Stiffness of carotid artery wall material and blood pressure in humans: application to antihypertensive therapy and stroke prevention. *Stroke* **2000,** 31(3), 782–790.
5. Motomiya, M., Karino, T., Flow patterns in the human carotid artery bifurcation. *Stroke* **1984,** 15(1), 50–56.
6. Lehoux, S., Castier, Y., Tedgui, A., Molecular mechanisms of the vascular responses to haemodynamic forces. *J Intern Med* **2006,** 259(4), 381–392.
7. Wung, B. S., Cheng, J. J., Shyue, S. K., Wang, D. L., NO modulates monocyte chemotactic protein-1 expression in endothelial cells under cyclic strain. *Arterioscler Thromb Vasc Biol* **2001,** 21(12), 1941–1947.
8. Oyre, S., Ringgaard, S., Kozerke, S., Paaske, W. P., Erlandsen, M., Boesiger, P., Pedersen, E. M., Accurate noninvasive quantitation of blood flow, cross-sectional lumen vessel area and wall shear stress by three-dimensional paraboloid modeling of magnetic resonance imaging velocity data. *J Am Coll Cardiol* **1998,** 32(1), 128–134.

9. Yim, P., Demarco, K., Castro, M. A., Cebral, J., Characterization of shear stress on the wall of the carotid artery using magnetic resonance imaging and computational fluid dynamics. *Stud Health Technol Inform* **2005,** 113, 412–442.

10. Younis, H. F., Kaazempur-Mofrad, M. R., Chan, R. C., Isasi, A. G., Hinton, D. P., Chau, A. H., Kim, L. A., Kamm, R. D., Hemodynamics and wall mechanics in human carotid bifurcation and its consequences for atherogenesis: investigation of inter-individual variation. *Biomech Model Mechanobiol* **2004,** 3(1), 17–32.